Triplet-state transitions in beryllium: Accurate energies and oscillator strengths

Saeed Nasiri [1,*] Ludwik Adamowicz [2,3,4,†] and Sergiy Bubin [1,‡]

[1]*Department of Physics, Nazarbayev University, Astana 010000, Kazakhstan*

[2]*Department of Chemistry and Biochemistry, University of Arizona, Tucson, Arizona 85721, USA*

[3]*Department of Physics, University of Arizona, Tucson, Arizona 85721, USA*

[4]*Hylleraas Centre for Quantum Molecular Sciences, Department of Chemistry, University of Oslo, N-0315 Oslo, Norway*

(Received 28 April 2025; accepted 3 November 2025; published 4 December 2025)

We present highly accurate variational calculations of triplet excited states of the beryllium atom using all-electron explicitly correlated Gaussian basis sets. The employed approach that treats the electrons and the nucleus on the same footing enables precise determination of the energy spectrum, wave functions, and transition properties of low-lying $^3S^e$ and $^3P^o$ states of the naturally occurring ^{9}Be isotope and the model $^\infty$Be system. Benchmark-quality total and transition energies, as well as oscillator strengths determined in both the length and velocity gauges, are reported. The results are compared with available theoretical and experimental data. The comparison shows excellent agreement of the present results with the experiment. They also provide refinement for the values where discrepancies had existed before.

DOI: 10.1103/qrtf-56np

I. INTRODUCTION

The electronic structure of many-electron atomic and molecular systems is inherently complex, making it nearly impossible to measure all relevant properties—such as transition energies, fine structure splitting, and oscillator strengths—at a uniformly high level of accuracy. The challenge achieving of such a level has persisted even for small atomic and molecular species that play a crucial role in such fields as astrophysics [1,2] or high-resolution spectroscopy [3–5]. Consequently, accurate theoretical studies are indispensable, particularly for smaller systems with only a few electrons, where high-precision calculations are feasible. Computing the spectral properties requires solving the Schrödinger equation to determine ground and excited states of the system. However, as Dirac famously noted, "the difficulty is that the exact application of the physical laws leads to equations too complex to solve" [6]. Thus, practical calculations of the spectral properties of atoms and molecules must rely on approximate numerical solutions.

For few-electron systems, the most effective approach for the calculations currently relies on the variational method, where the wave function is expanded in terms of explicitly correlated basis functions, i.e., basis functions that explicitly depend on all interparticle distances.

While this method is computationally demanding, it consistently delivers the needed highest precision for systems containing up to six to eight identical particles. These particles can be either electrons or nuclei, or both. As a result, it remains the preferred choice whenever achieving maximum accuracy is of paramount importance.

When it comes to choosing basis functions for explicitly correlated variational calculations, the two most commonly adopted choices are the Hylleraas-type (Hy) functions and the explicitly correlated Gaussian (ECG) functions. The Hy functions can yield highly converged results for systems containing up to three identical particles (electrons). For example, the computed nonrelativistic energies of the helium atom achieve the accuracy that exceeds a femtohartree (for a review on this topic see Ref. [7]). However, the Hy functions, despite their superb accuracy, cannot be easily extended to study states of a system with more than three electrons. The ECG basis functions do not have this limitation. However, they are not as efficient as the Hy functions in describing the behavior of the wave function near the particle coalescence points and also have less favorable long-range behavior [8]. The deficiency of the ECG basis functions of not exact fulfilling the Kato cusp conditions [9,10] can be effectively remedied by using larger expansions of the wave function in terms of these basis functions.

Employing ECGs in the high-accuracy calculation necessitates extensive optimization of the these functions for each studied states. Multiple studies carried out by the present authors have demonstrated that the basis-set optimization is by far the most time-consuming part of the calculations [11]. It is important to note that in our variational ECG calculations, the nonlinear parameters of the Gaussians are optimized using a procedure which employs the analytically computed gradient of the energy determined with respect to these parameters [12–14]. This capability has significantly accelerated the process of the wave function generation, enabling us to investigate larger atomic and molecular systems in ground and excited (in some cases even highly excited) states.

Recently, we have performed high-precision ECG calculations for several small neutral atoms [15–20] and ions [21,22] involving determination of transition properties, fine-structure splittings, and leading-order relativistic and quantum

*Contact author: saeed.nasiri@nu.edu.kz

†Contact author: ludwik@arizona.edu

‡Contact author: sergiy.bubin@nu.edu.kz

 ©2025 American Physical Society

electrodynamics (QED) corrections to the energy levels. These studies have demonstrated high effectiveness of the ECG wave functions in achieving benchmark accuracy for atomic systems. Building on these advancements, the aim of the present work is to investigate the $1s^2\,2s\,np\,{}^3P$ ($n = 2-11$) and $1s^2\,2s\,ns\,{}^3S$ ($n = 3-12$) states of the beryllium atom.

Despite their fundamental importance for understanding the electronic structure of few-electron systems, the triplet-state manifold of neutral beryllium has received surprisingly little attention in the literature. While Be is the simplest open-shell four-electron system, accurate theoretical data for its $1s^2 2s\,np\,{}^3P$ and $1s^2 2s\,ns\,{}^3S$ states are scarce. These states offer a stringent test of explicitly correlated methods because they combine a compact three-electron core with a diffuse Rydberg electron—an ideal stage for examining electron-electron correlation and mass-polarization effects beyond the closed-shell paradigm. On the experimental side, accurate experimental data for the triplet states have long remained scarce in part due to the challenges associated with working with beryllium (its toxicity has hindered extensive laboratory spectroscopy [23]). Only recently have new spectroscopic measurements of the Be triplet series begun to emerge, helping to fill up this gap in our knowledge (e.g., high-precision laser spectroscopy measurements are now underway [24]). The scarcity of the existing data underlines the need for reliable theoretical and experimental benchmarks. In particular, accurate ($^3S \rightarrow {}^3P$) oscillator strengths (f_{if}) for the neutral Be, which feed directly into the modeling and interpretation of a range of applications, are missing. Such data, beyond intrinsic atomic-physics interest, are used in fusion-plasma applications. In those applications, beryllium is used as the main chamber (first-wall) material in the ITER-Like Wall at JET and is likewise foreseen for the ITER first wall [23], making Be a dominant intrinsic impurity in such devices [25]. Be I/Be II emission; e.g., the Be I line near 457 nm is routinely monitored to gauge beryllium erosion and edge-plasma conditions at JET. Quantitative analyses of these diagnostics depend on accurate transition probabilities and oscillator strengths, which enter the photon-emissivity coefficients used in collisional-radiative modeling tools such as ADAS [26]. In magnetic-confinement fusion, reliable oscillator strengths for key Be I triplet transitions (e.g., $2\,{}^3P \rightarrow 3\,{}^3S$) and adjacent lines are essential for predicting line emissivities, radiative power losses, and impurity transport inferred from edge-plasma spectroscopy [27,28]. By providing improved Be I oscillator strengths (with internal consistency checks), our results may reduce uncertainties in impurity concentrations, radiated power-loss calculations, and plasma-emissivity predictions for Be-walled devices.

It is also important to mention that Be is a candidate for precision tests of many-body QED and isotope-shift studies that probe nuclear-structure effects [29], connecting light-atom theory to metrological and astrophysical applications. By providing benchmark-quality nonrelativistic energies and oscillator strengths for the triplet series, our work establishes a reference dataset for both experimental spectroscopy and high-order relativistic/QED corrections. Note that our calculations explicitly incorporate recoil effects by employing a Hamiltonian that explicitly depends on the nuclear mass. They bridge the gap between the well-studied singlet states of Be and the open-shell triplet manifolds of heavier few-electron atoms, offering a new testing ground for correlated-wave-function theory.

We hope the results presented in this study will contribute to the broader effort of improving atomic structure theory and of refining our understanding of few-electron systems.

II. METHOD

A. Nonrelativistic nuclear-mass-dependent Hamiltonian

In the present nonrelativistic variational calculations of the beryllium atom, we first separate out the translational motion of the system as a whole from the internal motion. The corresponding internal Hamiltonian representing the internal motion is obtained by separating out the atom's center-of-mass motion from the nonrelativistic laboratory-frame Hamiltonian. This separation yields an "internal" Hamiltonian which is used in the present calculations. The separation is rigorous and results in the reduction the N-particle problem ($N = 5$ for the beryllium atom comprising four electrons and a nucleus) to an n-pseudoparticle problem ($n = N - 1 = 4$) represented by the internal Hamiltonian expressed in terms of the internal Cartesian coordinates, $\boldsymbol{r}_i$'s. In the present approach, the internal coordinates are defined as the position vectors of the electrons relative to the nucleus, which acts as the reference point. The internal nonrelativistic Hamiltonian, expressed in atomic units, is given by

$$\mathcal{H}_{\rm nr}^{\rm int} = -\frac{1}{2}\left(\sum_{i=1}^{n}\frac{1}{\mu_i}\nabla_{\boldsymbol{r}_i}^2 + \sum_{i=1}^{n}\sum_{j\neq i}^{n}\frac{1}{m_0}\nabla_{\boldsymbol{r}_i}'\nabla_{\boldsymbol{r}_j}\right) + \sum_{i=1}^{n}\frac{q_0 q_i}{r_i} + \sum_{i=1}^{n}\sum_{j<i}^{n}\frac{q_i q_j}{r_{ij}}. \tag{1}$$

Here $q_0 = 4$ is charge of the nucleus, $q_i = -1$ ($i = 1, \ldots, 4$) are the electron charges, m_0 is the nuclear mass ($m_0 = 16\,424.2055 m_e$ for ^{9}Be [30]; $m_0 = \infty$ for $^\infty$Be), $\mu_i = m_0 m_i/(m_0 + m_i)$ is the reduced mass of the ith electron ($m_i = 1$, $i = 1, \ldots, 4$), r_i is the distance between the ith electron and the nucleus, and $r_{ij} = |\boldsymbol{r}_j - \boldsymbol{r}_i|$ is the distance between electrons i and j. The prime symbol ($'$) stands for the vector/matrix transpose.

The computations involving the nonrelativistic Hamiltonian, $\mathcal{H}_{\rm nr}^{\rm int}$, can be performed for both finite and infinite nuclear mass. These calculations provide the nonrelativistic ground- and excited-state energies, $E_{\rm nr}$, along with the corresponding wave functions. Consequently, both the energy and wave function exhibit dependence on the nuclear mass. In the subsequent sections, we present results for both finite and infinite nuclear mass cases.

B. Basis functions

The basis functions in the form of of all-electron explicitly correlated Gaussians are used in the present calculations to construct the spatial part of the wave function for the S and P states considered in this work. They have the following form:

$$S\text{-type ECG:}\quad \phi_k^{(S)}(\boldsymbol{r}) = \exp[-\boldsymbol{r}'(A_k \otimes \mathrm{I})\boldsymbol{r}], \tag{2}$$

$$P\text{-type ECG:}\quad \phi_k^{(P)}(\boldsymbol{r}) = z_{i_k}\exp[-\boldsymbol{r}'(A_k \otimes \mathrm{I})\boldsymbol{r}], \tag{3}$$

where

$$\boldsymbol{r} = \begin{pmatrix} \boldsymbol{r}_1 \\ \vdots \\ \boldsymbol{r}_n \end{pmatrix} \tag{4}$$

is a $3n$-component column vector consisting of n internal coordinate vectors stacked upon each other, A_k is an $n \times n$ positive definite real symmetric matrix that is unique for each basis function, and I is a 3×3 identity matrix. The $\otimes$ symbol denotes the Kronecker product. The positive definiteness of A_k is required for ensuring that the basis function remains square integrable.

The P-type ECGs in Eq. (3) contain an additional prefactor before the Gaussian exponent. The z_{i_k} is the z coordinate of the ith electron, while i_k is the electron label, which can vary in the $(1, \ldots, n)$ range. i_k represents an adjustable integer parameter in the calculations. This parameter is specific to each basis function and its value is determined variationally (i.e., based on how well the energy is improved) when the function is first added to the basis set. The z_{i_k} is a Cartesian spherical-harmonic angular prefactor that generates basis functions corresponding to the definite values of the total orbital angular momentum ($L = 1$) and its projection on the z axis ($M_L = 0$). A proper ($L = 1, M_L = 0$) ECG is obtained regardless of the value of electron-label index i_k. Treating i_k as a variational parameter and optimizing it is optional because, due to indistiguishability of the electrons, choosing a fixed value of i_k (e.g., $i_k = 1$) and not optimizing it, but only optimizing the nonlinear exponential parameters (the elements of matrices A_k), should, in principle, lead to the same outcome provided the optimization process is thorough and yields the global minimum. For more information on the ECG basis sets used in high-accuracy atomic calculations see Refs. [8,11,31].

C. Oscillator strengths

In this work, we calculate the absorption oscillator strengths in both the length (L) and velocity (V) gauges. For a transition $|\psi_i\rangle \to |\psi_f\rangle$ between initial (i) and final (f) state, they are expressed as follows [4,32,33]:

$$f_{if}^{\mathrm{L}} = \frac{2}{3g_i} \Delta E_{if} \left|\boldsymbol{\mu}_{if}^{\mathrm{L}}\right|^2, \quad \left|\boldsymbol{\mu}_{if}^{\mathrm{L}}\right|^2 = |\langle\psi_i|\boldsymbol{\mu}^{\mathrm{L}}|\psi_f\rangle|^2 \tag{5}$$

and

$$f_{if}^{\mathrm{V}} = \frac{2}{3\, g_i\, \Delta E_{if}} \left|\boldsymbol{\mu}_{if}^{\mathrm{V}}\right|^2, \quad \left|\boldsymbol{\mu}_{if}^{\mathrm{V}}\right|^2 = |\langle\psi_i|\boldsymbol{\mu}^{\mathrm{V}}|\psi_f\rangle|^2, \tag{6}$$

respectively, where $g_i = 2J_i + 1$ is the statistical weight of the initial level (J_i is the total angular momentum quantum number), $\Delta E_{if} = E_f - E_i$ is the nonrelativistic transition energy between the initial state ψ_i and final state ψ_f, and $\boldsymbol{\mu}^{\mathrm{L}}$ and $\boldsymbol{\mu}^{\mathrm{V}}$ are the transition dipole operators in the length and velocity gauges, respectively. The transition dipole moment matrix elements associated with the $|\psi_i\rangle \to |\psi_f\rangle$ transition in both the length and velocity gauges can be written in the following form:

$$\begin{aligned} |\boldsymbol{\mu}_{if}|^2 &= |\langle\psi_i|\boldsymbol{\mu}|\psi_f\rangle|^2 \\ &= |\langle\psi_i|\mu_x|\psi_f\rangle|^2 + |\langle\psi_i|\mu_y|\psi_f\rangle|^2 + |\langle\psi_i|\mu_z|\psi_f\rangle|^2 \end{aligned} \tag{7}$$

Note that only the matrix elements between the ($L = 0, M_L = 0$) and ($L = 1, M_L = 0$) states need to be evaluated. This is possible because of the symmetry (one can obtain the transition dipole moment matrix elements $\boldsymbol{\mu}_{if}$ involving $L = 1$ final states corresponding to nonzero M_L values if the matrix element for the $M_L = 0$ value is known). The formulas for oscillator strengths and transition dipole matrix elements are provided in the Appendix. Specifically, the $|\boldsymbol{\mu}_{if}|^2$ values reported in the next section come from Eq. (A10).

For an n-electron atom or, in general, for a Coulomb system with arbitrary charges $(q_0, \ldots, q_n)$ and masses $(m_0, \ldots, m_n)$, the expressions for the transition dipole moments with respect to the origin located at the center of mass have the following form in the internal coordinates [34,35]:

$$\boldsymbol{\mu}^{\mathrm{L}} = \sum_{i=1}^{n} \left(q_i - \frac{m_i}{m_{\mathrm{tot}}} q_{\mathrm{tot}}\right) \boldsymbol{r}_i \tag{8}$$

and

$$\boldsymbol{\mu}^{\mathrm{V}} = \sum_{i=1}^{n} \left(\frac{q_0}{m_0} - \frac{q_i}{m_i}\right) \boldsymbol{p}_i, \tag{9}$$

where $\boldsymbol{p}_i = -i\,\nabla_{\boldsymbol{r}_i}$, $q_{\mathrm{tot}} = \sum_{i=0}^{n} q_i$ is the total charge of the system (zero for a neutral atom), and $m_{\mathrm{tot}} = \sum_{i=0}^{n} m_i$ is the total mass of the system. It should be noted that the above expressions for $\boldsymbol{\mu}^{\mathrm{L}}$ and $\boldsymbol{\mu}^{\mathrm{V}}$ are consistent with the Thomas-Reiche-Kuhn sum rule,

$$\sum_f f_{if} = n, \tag{10}$$

for any values of the charges and masses of the constituent particles. Therefore, they are valid for both the ^{9}Be isotope and infinitely heavy $^\infty$Be model atom that we consider in this work.

As mentioned, due to the dependence of the internal Hamiltonian (1) on the nuclear mass, the wave functions of the initial (ψ_i) and final (ψ_f) states also carry over the dependence on the nuclear mass. Thus, the wave functions for ^{9}Be and $^\infty$Be are slightly different. Consequently, the mass effect is included in the oscillator strength calculations because both the transition dipole moments ($|\boldsymbol{\mu}_{if}^{\mathrm{L}}|^2$ or $|\boldsymbol{\mu}_{if}^{\mathrm{V}}|^2$) and the nonrelativistic transition energy ΔE_{if} are mass dependent. This dependency on the nuclear mass will be elucidated in details in Sec. III.

III. RESULTS

A. Computational details

In the present study we investigate the lowest ten Rydberg ^3P ($1s^2\, 2s\, np\; n = 2, \ldots, 11$) states and the lowest ten Rydberg ^3S ($1s^2\, 2s\, ns\; n = 3, \ldots, 12$) states of the beryllium atom. In the first step of the calculations, the nonrelativistic wave functions and the corresponding energies for the considered states are calculated using the standard Rayleigh-Ritz variational method. To construct the ECG basis set for each state, the internal Hamiltonian corresponding to ^{9}Be is employed [see Eq. (1)]. The basis sets generated for all the considered states of ^{9}Be are then used to compute the energies and corresponding wave functions for $^\infty$Be. Since the wave

function differences between isotopes are rather small, it is unnecessary to reoptimize the nonlinear parameters of the gaussians for each isotope individually. Adjusting the linear variational parameters by solving the generalized eigenvalue problem independently for each isotope turns out to be sufficient for capturing the differences accurately.

The present calculations were carried out on three different computer clusters, each equipped with AMD EPYC 7642, AMD EPYC 7502, and Intel Xeon E5-2695v3 CPUs, utilizing several hundred CPU cores simultaneously. The computations have been performed over a span of more than a year, with most CPU time dedicated to expanding the basis set and optimizing the nonlinear parameters of the Gaussians. The basis set was independently generated for each of the beryllium atom states, reaching a size of 15 000 ECGs. The optimization approach is detailed in Refs. [15,17,18,36].

Our code, written in FORTRAN, leverages the MPI (Message Passing Interface) library to enable parallel processing. Most calculations are performed using extended precision (also known as extended double precision or fp80), representing floating-point numbers with 80 bits of data (in contrast to 64 bits for standard double precision, fp64). Although extended precision calculations are slower (by approximately a factor of 5), they enhance optimization quality and ensure significantly improved numerical stability, particularly when handling large basis sets for excited states.

B. Nonrelativistic energies

Table I presents the results of nonrelativistic variational calculations for the lowest ten Rydberg ^3P and the lowest ten Rydberg ^3S states of the beryllium atom. The calculations utilize ECG expansions of the wave functions and the internal Hamiltonian (1). In the table, two values are provided for each state: the first represents the variational energies computed using a basis set of 14 000 or 15 000 ECGs, while the second corresponds to the extrapolated energy obtained from the energies calculated with basis sets ranging in size from 10 000 to 15 000 ECGs.

Over the past two decades, our experience with ECG calculations has shown that expanding the basis set by linearly increasing the number of ECG functions often results in energy increments that follow a geometric progression. Consequently, we apply a geometric progression approximation to extrapolate the results to the infinite basis set limit. For further details, we refer to our previous publications [18,36].

As one can see, the number of the significant figures shown in the energy values for each state decreases with the level of excitation. This reflects the slowing of the energy convergence rate with the basis size as the wave function becomes more complicated and has more radial nodes. This is illustrated in Fig. 1, where we plot the nucleus-electron pair correlation function for one of the upper S states we computed. The pair correlation function is defined as $g_i(\boldsymbol{\xi}) = \langle \delta(\boldsymbol{r}_i - \boldsymbol{\xi}) \rangle$, where $i = 1, \ldots, n$. The $g_i(\boldsymbol{\xi})$ function represents the probability density of particles 1 (the nucleus) and $i + 1$ (an electron) to be found at a distance ξ from each other. For Rydberg-like excitations, the probability density becomes progressively more extended in space due to the fourth, outer electron. Figure 1 illustrates $g_i(\boldsymbol{r})$ for the excited $1s^2 2s 11s$ (^3S) state. It is evident that the probability density of finding an electron extends far from the nucleus, with a pronounced peak around $r \approx 200$ a.u. For the purpose of comparison, in the same figure we show the same pair correlation function for the $11s$ state of a hydrogen-like atom with an effective nuclear mass $m(^9\mathrm{Be}) + 3m_e$ and charge $+1$ as well as for the singlet $1s^2 2s 11s$ (^1S) state of ^{9}Be. As can be seen in the figure, the correlation function for $11\,^3S$ state of beryllium closely resembles the one for a hydrogen-like atom and is somewhat more contracted. This can be attributed to diffuseness of the three-electron core that the outer electron interacts with and the effective repulsion due to the exchange interaction that is absent in the hydrogen-like atom.

As mentioned earlier, most previously reported transition energies and transition intensities are derived from mean-field calculations, although there are a few studies on the lowest states of beryllium that employ ECG basis functions [16,37,38,40]. Both the employed ECG basis sets and the number of considered states in this work are significantly larger than in the previous studies. For instance, 6144 and 7000 ECGs were used in the wave function expansion for the ^3P and ^3S states, respectively, in Refs. [37,40]. In contrast, the present study employs up to 15 000 ECGs in the calculations. Consequently, the computed variational nonrelativistic energies are notably lower than those obtained in the aforementioned works.

Besides the explicitly correlated methods, the lower part of the spectrum of the beryllium atom has been calculated using other *ab initio* approaches such as configuration interaction method (CI) [38] and full-core plus correlation method (FCPC) [39]. The n^3P states (up to $n = 8$ only) of the beryllium atom were previously computed with high accuracy in Ref. [16], where the ECG basis sets containing up to 10 000 functions were used. In the present study we employed 15 000 ECGs. Interestingly, the total energies reported in Ref. [16] are slightly lower, i.e., they are marginally better converged, even though the number of ECGs is smaller. At first glance one might think that the present calculations were performed with a less thorough optimization of the Gaussian nonlinear parameters. However, this is not the case. The marginally slower rate of convergence should be be attributed to using a different form of the Young projection operator for constructing the spatial wave function in the spin-free formalism [42]. In the present work, the Young operator is taken as $\mathcal{Y} = \mathcal{SA}$, where $\mathcal{S}$ is a symmetrizer over all rows and $\mathcal{A}$ is an antisymmetrizer over all columns of the corresponding Young tableau. In contrast, in Ref. [16] the form of the Young operator was $\mathcal{Y} = \mathcal{AS}$. It has been verified that both yield the same energies and expectation values in the limit of the infinite basis set size. However, their convergence behavior differs. Specifically, it was found that for high-spin (e.g., triplet) states $\mathcal{Y} = \mathcal{AS}$ ordering exhibits a somewhat faster convergence rate.

The main objective of the present work is to calculate the oscillator strengths for all transitions between the considered ^3S and ^3P states of the stable beryllium isotope (^{9}Be) and a beryllium atom with infinite nuclear mass ($^\infty$Be). The oscillator strengths are computed at the nonrelativistic level of theory. Due to the presence of the nuclear mass in the internal Hamiltonian, Eq. (1), used in the calculations, nuclear mass effects are explicitly incorporated into the calculated

TABLE I. Convergence of the nonrelativistic energies of the $1s^2\ 2s\ np\ (n\ ^3P)$ and $1s^2\ 2s\ ms\ (m\ ^3S)$ states ($n = 2, \ldots, 11$; $m = 3, \ldots, 12$) of ^{9}Be and $^\infty$Be atoms with the number of ECG basis functions. All values are in atomic units.

State	Method	Ref.	Basis	^{9}Be	$^\infty$Be
$2\ ^3P$	ECG	This work	15 000	−14.566 341 477 7	−14.567 244 225 4
	ECG	This work	∞	−14.566 341 481 4(61)	−14.567 244 231 5(61)
	ECG	[16]	9000	−14.566 341 480	−14.567 244 230
	ECG	[37]	6144		−14.567 244 215 84
	ECG	[37]	∞		−14.567 244 232(8)
	CI[a]	[38]	$l_{\max} = 6$		−14.565 365
	FCPC[b]	[39]			−14.567 238 30
$3\ ^3S$	ECG	This work	14 000	−14.429 160 992 2	−14.430 067 702 5
	ECG	This work	∞	−14.429 160 993 2(10)	−14.430 067 703 6(10)
	ECG	[37]	4096		−14.430 067 666 35
	ECG	[37]	∞		−14.430 067 678(7)
	ECG	[38]			−14.430 060 025
	ECG	[40]	7000		−14.430 059 43
	CI[a]	[38]	$l_{\max} = 6$		−14.428 858
	FCPC[b]	[39]			−14.429 798 54
$3\ ^3P$	ECG	This work	15 000	−14.398 065 860 0	−14.398 968 688 1
	ECG	This work	∞	−14.398 065 867 8(88)	−14.398 968 696 9(88)
	ECG	[16]	9000	−14.398 065 863	−14.398 968 692
	CI[a]	[38]	$l_{\max} = 6$		−14.395 471
	FCPC[b]	[39]			−14.398 960 12
$4\ ^3S$	ECG	This work	14 000	−14.372 550 833 3	−14.373 453 730 7
	ECG	This work	∞	−14.372 550 835 7(24)	−14.373 453 733 1(24)
	CI[a]	[38]	$l_{\max} = 6$		−14.371 277
	ECG	[38]			−14.372 858 590
$4\ ^3P$	ECG	This work	15 000	−14.362 049 938	−14.362 951 443
	ECG	This work	∞	−14.362 049 947(11)	−14.362 951 452(11)
	ECG	[16]	9000	−14.362 049 944	−14.362 951 448
	CI[a]	[38]	$l_{\max} = 6$		−14.357 02
	FCPC[b]	[41]			−14.362 48
$5\ ^3S$	ECG	This work	15 000	−14.352 031 551 5	−14.352 933 069 0
	ECG	This work	∞	−14.352 031 557 9(80)	−14.352 933 075 4(80)
	CI[a]	[38]	$l_{\max} = 6$		−14.345 918
	ECG	[38]			−14.351 112 52
$5\ ^3P$	ECG	This work	15 000	−14.347 224 119	−14.348 124 983
	ECG	This work	∞	−14.347 224 138(20)	−14.348 125 001(20)
	ECG	[16]	10 000	−14.347 224 130	−14.348 124 994
$6\ ^3S$	ECG	This work	15 000	−14.342 234 513	−14.343 135 379
	ECG	This work	∞	−14.342 234 535(25)	−14.343 135 402(25)
	ECG	[38]			−14.337 598 15
$6\ ^3P$	ECG	This work	15 000	−14.339 637 411	−14.340 537 919
	ECG	This work	∞	−14.339 637 469(65)	−14.340 537 977(65)
	ECG	[16]	10 000	−14.339 637 441	−14.340 537 949
$7\ ^3S$	ECG	This work	15 000	−14.336 791 29	−14.337 691 80
	ECG	This work	∞	−14.336 791 41(12)	−14.337 691 92(12)
	ECG	[38]			−14.328 903 15
$7\ ^3P$	ECG	This work	15 000	−14.335 230 89	−14.336 131 18
	ECG	This work	∞	−14.335 230 99(13)	−14.336 131 28(13)
	ECG	[16]	10 000	−14.335 230 949	−14.336 131 240
$8\ ^3S$	ECG	This work	15 000	−14.333 454 17	−14.334 354 46
	ECG	This work	∞	−14.333 454 36(22)	−14.334 354 66(22)
$8\ ^3P$	ECG	This work	15 000	−14.332 444 17	−14.333 344 32
	ECG	This work	∞	−14.332 444 41(28)	−14.333 344 56(28)
	ECG	[16]	10 000	−14.332 444 254	−14.333 344 405

TABLE I. (*Continued.*)

State	Method	Ref.	Basis	^{9}Be	$^{\infty}$Be
$9\,^3S$	ECG	This work	15 000	−14.331 260 40	−14.332 160 55
	ECG	This work	∞	−14.331 260 89(65)	−14.332 161 04(65)
$9\,^3P$	ECG	This work	15 000	−14.330 569 1	−14.331 469 1
	ECG	This work	∞	−14.330 570 5(19)	−14.331 469 7(19)
	ECG	[16]	10 000	−14.330 569 664	−14.331 469 717
$10\,^3S$	ECG	This work	15 000	−14.329 739 2	−14.330 639 2
	ECG	This work	∞	−14.329 742 5(36)	−14.330 642 6(36)
$10\,^3P$	ECG	This work	15 000	−14.329 245 1	−14.330 145 1
	ECG	This work	∞	−14.329 247 9(48)	−14.330 148 3(49)
$11\,^3S$	ECG	This work	15 000	−14.328 637 7	−14.329 537 7
	ECG	This work	∞	−14.328 643 1(58)	−14.329 543 1(58)
$11\,^3P$	ECG	This work	15 000	−14.328 275 0	−14.329 174 9
	ECG	This work	∞	−14.328 280 0(57)	−14.329 179 9(58)
$12\,^3S$	ECG	This work	16 000	−14.327 808	−14.328 708
	ECG	This work	∞	−14.327 817(15)	−14.328 716(15)

[a]Configuration interaction (CI) method using ≈ 2000 configurations and Slater orbitals.
[b]Full-core plus correlation method.

total energies and transition energies. In Table II we present the nuclear-mass-dependent transition energies expressed in wave numbers obtained in this work. The hartree-to-cm^{-1} conversion factor adopted in this study is 219 474.631 363 14 [43]. Note that the extrapolated transition energies and the corresponding uncertainties were determined by analyzing the convergence patterns of $E_f - E_i$ rather than extrapolating E_f and E_i independently and taking the uncertainty as a root mean square of the individual uncertainties of E_i and E_f. This is justified because the uncertainties of E_f and E_i are partially correlated as both E_f and E_i represent variational upper bounds, which leads to a partial cancellation of errors when computing the difference. The uncertainties due to basis set truncation are small (less than 0.01 cm^{-1}) for transitions involving lower states but increase in magnitude for higher states. Because relativistic and higher order QED corrections are not included in the transition energies, their accuracy cannot be directly benchmarked through comparison with available experimental data.

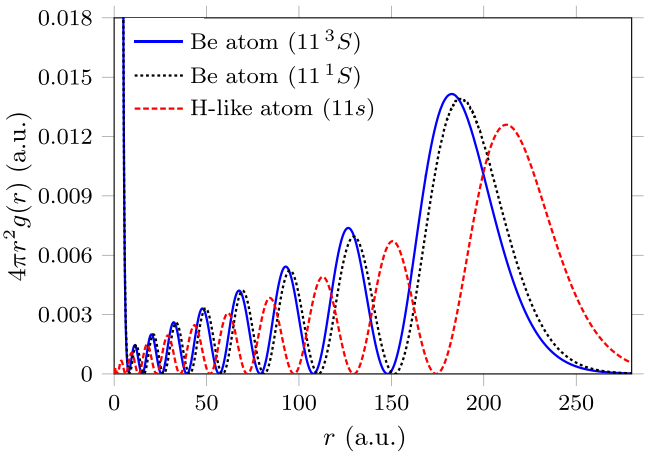

FIG. 1. Nucleus–electron pair correlation functions for the $11\,^3S$ state of ^{9}Be in comparison with the $11\,^1S$ state of ^{9}Be and the $11s$ state of the hydrogen-like atom with the effective nuclear mass of $m_0 = m(^9\text{Be}) + 3m_e$.

C. Oscillator strengths

Table III shows the convergence of oscillator strengths computed in the length and velocity gauges as a function of the ECG basis set size for three representative transitions. The data illustrate the convergence pattern observed across all transitions considered in this study. The computed values exhibit very good convergence for the lower-energy transitions. For instance, the oscillator strengths in the length and velocity gauges for the $2\,^3P \rightarrow 3\,^3S$ transition converge to six significant figures. This level of precision surpasses previously reported results by several orders of magnitude [39,44–53].

In all previous studies, only the transitions between the low-lying S and P states have been considered. Thus, for transitions involving higher states, the oscillator strengths calculated in this work are the first-ever results obtained in direct calculations. It is worth noting that the most accurate previous calculations of the beryllium oscillator strengths were performed using mean-field approaches. Among these, two studies stand out as particularly comprehensive. The first, by Tachiev and Froese Fischer [52], employed the multi-configuration Hartree-Fock (MCHF) method to compute theoretical lifetimes for selected $n\,^3P$ and $m\,^3S$ states up to $n = 4$ and $m = 7$. The second, by Chen [46], utilized a model-potential method with the B-spline CI approach that incorporates a semiempirical core potential (BCICP). The values reported in the two studies match within their estimated (and relatively large) uncertainty the values obtained in the present work. For example, the values $8.213\,700(39) \times 10^{-2}$ and $8.213\,698(27) \times 10^{-2}$ are obtained in the present work for the $2\,^3P \rightarrow 3\,^3S$ transition using the length and velocity gauges, respectively. These values agree well with the

TABLE II. Nonrelativistic absorption transition energies ($\Delta E_{\rm nr}$) for the lowest ten ^3P and ten ^3S states of the beryllium atom (^{9}Be and $^\infty$Be). All values are in cm^{-1}. The uncertainty estimates due to the extrapolation are shown in parentheses.

Transition	^{9}Be	$^\infty$Be	Transition	^{9}Be	$^\infty$Be
$2\,^3P \to 3\,^3S$	30 107.6369(18)	30 106.7677(18)	$3\,^3S \to 3\,^3P$	6824.5907(22)	6825.4426(22)
$3\,^3S \to 4\,^3P$	14 729.1719(80)	14 730.3144(80)	$3\,^3S \to 5\,^3P$	17 983.062(15)	17 984.345(15)
$3\,^3S \to 6\,^3P$	19 648.150(14)	19 649.511(14)	$3\,^3S \to 7\,^3P$	20 615.276(61)	20 616.685(61)
$3\,^3S \to 8\,^3P$	21 226.87(16)	21 228.31(16)	$3\,^3S \to 9\,^3P$	21 638.35(66)	21 639.81(66)
$3\,^3S \to 10\,^3P$	21 928.5(42)	21 929.9(42)	$3\,^3S \to 11\,^3P$	22 140.8(13)	22 142.3(13)
$2\,^3P \to 4\,^3S$	42 532.1308(13)	42 532.0985(13)	$3\,^3P \to 4\,^3S$	5599.9016(12)	5599.8866(12)
$4\,^3S \to 4\,^3P$	2304.6795(73)	2304.9852(73)	$4\,^3S \to 5\,^3P$	5558.570(15)	5559.016(15)
$4\,^3S \to 6\,^3P$	7223.657(13)	7224.181(13)	$4\,^3S \to 7\,^3P$	8190.781(61)	8191.352(61)
$4\,^3S \to 8\,^3P$	8802.34(16)	8802.95(16)	$4\,^3S \to 9\,^3P$	9213.86(66)	9214.48(66)
$4\,^3S \to 10\,^3P$	9504.2(42)	9504.8(42)	$4\,^3S \to 11\,^3P$	9716.6(9)	9717.3(9)
$2\,^3P \to 5\,^3S$	47 035.5929(14)	47 035.8634(14)	$3\,^3P \to 5\,^3S$	10 103.362 49(56)	10 103.650 32(56)
$4\,^3P \to 5\,^3S$	2198.7823(62)	2198.7794(62)	$5\,^3S \to 5\,^3P$	1055.109(13)	1055.252(13)
$5\,^3S \to 6\,^3P$	2720.193(13)	2720.415(13)	$5\,^3S \to 7\,^3P$	3687.315(59)	3687.584(59)
$5\,^3S \to 8\,^3P$	4298.93(16)	4299.23(16)	$5\,^3S \to 9\,^3P$	4710.42(66)	4710.74(66)
$5\,^3S \to 10\,^3P$	5000.8(42)	5001.1(42)	$5\,^3S \to 11\,^3P$	5213.5(9)	5213.8(9)
$2\,^3P \to 6\,^3S$	49 185.7917(53)	49 186.2051(53)	$3\,^3P \to 6\,^3S$	12 253.5621(38)	12 253.9928(38)
$4\,^3P \to 6\,^3S$	4348.9809(29)	4349.1210(29)	$5\,^3P \to 6\,^3S$	1095.0897(95)	1095.0889(95)
$6\,^3S \to 6\,^3P$	569.990(10)	570.069(10)	$6\,^3S \to 7\,^3P$	1537.110(56)	1537.236(56)
$6\,^3S \to 8\,^3P$	2148.72(16)	2148.87(16)	$6\,^3S \to 9\,^3P$	2560.22(66)	2560.40(66)
$6\,^3S \to 10\,^3P$	2850.4(42)	2850.6(42)	$6\,^3S \to 11\,^3P$	3063.17(90)	3063.37(90)
$2\,^3P \to 7\,^3S$	50 380.418(26)	50 380.910(26)	$3\,^3P \to 7\,^3S$	13 448.184(29)	13 448.694(29)
$4\,^3P \to 7\,^3S$	5543.602(30)	5543.821(30)	$5\,^3P \to 7\,^3S$	2289.714(27)	2289.792(27)
$6\,^3P \to 7\,^3S$	624.625(25)	624.625(25)	$7\,^3S \to 7\,^3P$	342.502(35)	342.549(35)
$7\,^3S \to 8\,^3P$	954.06(14)	954.14(14)	$7\,^3S \to 9\,^3P$	1365.53(64)	1365.63(64)
$7\,^3S \to 10\,^3P$	1655.7(41)	1655.8(41)	$7\,^3S \to 11\,^3P$	1868.35(93)	1868.48(93)
$2\,^3P \to 8\,^3S$	51 112.80(11)	51 113.34(11)	$3\,^3P \to 8\,^3S$	14 180.56(11)	14 181.11(11)
$4\,^3P \to 8\,^3S$	6275.96(10)	6276.22(10)	$5\,^3P \to 8\,^3S$	3022.03(13)	3022.16(13)
$6\,^3P \to 8\,^3S$	1356.93(13)	1356.98(13)	$7\,^3P \to 8\,^3S$	389.80(14)	389.80(14)
$8\,^3S \to 8\,^3P$	221.80(13)	221.84(13)	$8\,^3S \to 9\,^3P$	633.12(55)	633.18(55)
$8\,^3S \to 10\,^3P$	923.6(41)	923.6(41)	$8\,^3S \to 11\,^3P$	1136.16(79)	1136.24(79)
$2\,^3P \to 9\,^3S$	51 594.10(27)	51 594.67(27)	$3\,^3P \to 9\,^3S$	14 661.85(29)	14 662.43(29)
$4\,^3P \to 9\,^3S$	6757.26(29)	6757.56(29)	$5\,^3P \to 9\,^3S$	3503.30(36)	3503.46(36)
$6\,^3P \to 9\,^3S$	1838.19(39)	1838.27(39)	$7\,^3P \to 9\,^3S$	871.03(41)	871.07(41)
$8\,^3P \to 9\,^3S$	259.42(42)	259.42(42)	$9\,^3S \to 9\,^3P$	152.19(45)	152.22(45)
$9\,^3S \to 10\,^3P$	442.1(39)	442.1(39)	$9\,^3S \to 11\,^3P$	654.75(64)	654.80(64)
$2\,^3P \to 10\,^3S$	51 927.73(79)	51 928.33(79)	$3\,^3P \to 10\,^3S$	14 995.50(79)	14 996.11(79)
$4\,^3P \to 10\,^3S$	7090.90(78)	7091.22(78)	$5\,^3P \to 10\,^3S$	3837.00(77)	3837.18(77)
$6\,^3P \to 10\,^3S$	2171.91(78)	2172.01(78)	$7\,^3P \to 10\,^3S$	1204.54(80)	1204.59(80)
$8\,^3P \to 10\,^3S$	592.87(86)	592.89(86)	$9\,^3P \to 10\,^3S$	181.28(86)	181.28(86)
$10\,^3S \to 10\,^3P$	107.9(34)	107.4(34)	$10\,^3S \to 11\,^3P$	320.54(93)	320.57(93)
$2\,^3P \to 11\,^3S$	52 168.3(18)	52 168.9(18)	$3\,^3P \to 11\,^3S$	15 236.0(18)	15 236.6(18)
$4\,^3P \to 11\,^3S$	7331.3(19)	7331.7(19)	$5\,^3P \to 11\,^3S$	4077.3(20)	4077.5(20)
$6\,^3P \to 11\,^3S$	2412.1(22)	2412.2(22)	$7\,^3P \to 11\,^3S$	1444.5(27)	1444.5(27)
$8\,^3P \to 11\,^3S$	832.5(30)	832.5(30)	$9\,^3P \to 11\,^3S$	420.9(31)	420.9(31)
$10\,^3P \to 11\,^3S$	132.6(23)	132.8(23)	$11\,^3S \to 11\,^3P$	80.8(12)	80.8(12)
$2\,^3P \to 12\,^3S$	52 351.1(28)	52 351.7(28)	$3\,^3P \to 12\,^3S$	15 418.9(28)	15 419.5(28)
$4\,^3P \to 12\,^3S$	7514.0(27)	7514.3(27)	$5\,^3P \to 12\,^3S$	4259.8(29)	4260.0(29)
$6\,^3P \to 12\,^3S$	2594.8(28)	2594.9(28)	$7\,^3P \to 12\,^3S$	1627.4(30)	1627.5(30)
$8\,^3P \to 12\,^3S$	1015.7(32)	1015.7(32)	$9\,^3P \to 12\,^3S$	602.2(38)	603.6(38)
$10\,^3P \to 12\,^3S$	313.0(33)	313.2(33)	$11\,^3P \to 12\,^3S$	99.1(45)	99.1(45)

length-gauge result of $8.44(84) \times 10^{-2}$ obtained is the multi-configuration Hartree-Fock (MCHF) calculations [56] and the length-gauge value of 8.23×10^{-2} computed using the BCICP method [46]. While in neither of these two studies the uncertainties of the computed values were reported directly, Fuhr and Wiese [53] estimated the uncertainty of

TABLE III. Nonrelativistic multiplet absorption oscillator strengths in length (f^{L}) and velocity (f^{V}) gauges for some of the studied transitions obtained for the case of an infinite nuclear mass ($^{\infty}$Be). The oscillator strength uncertainties (given in parentheses) are computed as root mean squares of the uncertainties of $|\boldsymbol{\mu}_{if}^{\mathrm{L}}|^2$ or $|\boldsymbol{\mu}_{if}^{\mathrm{V}}|^2$ and ΔE_{if}, where ΔE_{if} is the difference between the nonrelativistic energies of the initial (i) and final (f) states.

Basis(S)	Basis(P)	f_{if}^{L}	f_{if}^{V}
		$2\,^3P \rightarrow 3\,^3S$	
10 000	10 000	0.082 136 18	0.082 137 12
12 000	12 000	0.082 136 35	0.082 137 12
14 000	14 000	0.082 136 61	0.082 137 25
∞	∞	0.082 137 00(39)	0.082 136 98(27)
CICP [44][a]		0.0821	
BCIBP [45][b]		0.0841	
BCICP [46][c]		0.0823	
TDGI [47,48][d]		0.0263	0.0256
FCPC [39][e]		0.0806	
CI [49]		0.083	
CICP [50]		0.0829	0.0855
PFCCI [51][f]		0.079	
MCHF [52,53][g]		0.0844(84)	
Experiment [54][h]		0.089(3)	
Experiment [55][i]		0.086(2)	
		$4\,^3S \rightarrow 8\,^3P$	
10 000	10 000	0.000 051 247	0.000 051 45
12 000	12 000	0.000 051 258	0.000 051 23
14 000	14 000	0.000 051 264	0.000 051 28
∞	∞	0.000 051 281(17)	0.000 051 37(23)
BCICP [46]		0.000 053 1	
		$11\,^3P \rightarrow 12\,^3S$	
10 000	10 000	1.248	1.117
12 000	12 000	1.246	1.140
14 000	14 000	1.239	1.155
15 000	15 000	1.240	1.167
∞	∞	1.220(66)	1.219(11)

[a]Configuration interaction (CI) with plus core polarization (CICP).
[b]B-spline CI calculations using a Briet-Pauli Hamiltonian (BCIBP).
[c]B-spline CI calculation with a semiempirical core potential (BCICP).
[d]Time-dependent gauge-invariant method (TDGI).
[e]Full-core plus correlation method (FCPC).
[f]Polarized frozen-core CI method (PFCCI).
[g]Multiconfiguration Hartree-Fock method (MCHF). The uncertainty is calculated based on procedure in Ref. [53].
[h]The lifetime of the state was measured in 1971. The particle beam was excited using carbon foils.
[i]The lifetime of the state was measured in 1980. The excitation was performed with a pulsed dye laser.

the MCHF results. All available estimated uncertainties for the prior results are shown in the tables where we make a comparison. Beyond the $2\,^3P \rightarrow 3\,^3S$ transition, a comparison of other computed values from the present work with those obtained using MCHF [53,56] and BCICP [46] suggests that the BCICP method yields results that are closer to ours. Tables IV and V present the calculated multiplet transition dipole-moment matrix elements and absorption oscillator strengths for the $S \rightarrow P$ and $P \rightarrow S$ transitions of ^{9}Be and of the beryllium atom with an infinite nuclear mass ($^{\infty}$Be). The oscillator strengths are computed for all states considered in this study. Only the extrapolated values obtained from the calculations with 10 000–15 000 ECGs are shown in the tables. The reported uncertainties account for errors arising from different sources: those in Table IV arise from the basis-set truncation, while those in Table V are determined as the root mean square of the uncertainties in $|\boldsymbol{\mu}_{if}|^2$ and in ΔE. The computed oscillator strengths are compared with available literature results to assess their accuracy and consistency.

As observed in Table V, the accuracy of the computed oscillator strengths decreases with the increase of the principal quantum numbers of the states involved in the transitions. This decline in accuracy can be attributed to two closely related factors. First, the nodal structure of the wave functions becomes increasingly complex and diffuse for highly excited states, making them progressively more difficult to describe accurately. Second, the transition dipole moment is primarily defined not by the electron density of the inner three-electron core but by the outer Rydberg electron, whose density extends far away from the nucleus. The outer electron's wave function and the precise position of its nodes for Rydberg-like states has progressively smaller impact on the value of the total energy (defined primarily by the core). Therefore they may not be particularly well refined in the process of the variational optimization of the total wave function [57]. At the same time, the transition dipole matrix elements remain extremely sensitive to the accuracy and quality of the outer electron's wave function. Further refinement and basis size increase could improve the accuracy of the wave function in the outer region, but it requires progressively larger computational effort.

A visual representation of oscillator strengths for all transitions considered in this work is given in Fig. 2, where we show the values for ^{9}Be obtained in the length gauge. As can be seen there, the largest oscillator strengths correspond to the transitions between S and P states with the same principal quantum number, i.e., the $n\,^3P \rightarrow n\,^3S$ transitions. It can also be noted that the calculated oscillator strengths between adjacent states ($n\,^3S \rightarrow n-1\,^2P$) are comparatively large in magnitude as well. This suggests the possibility of employing a $P \rightarrow S \rightarrow P \rightarrow S \rightarrow \cdots$ "cascade" excitation sequence to prepare a beryllium atom in a specific Rydberg state. The overall map of the oscillator strengths in the present work shows similarity (at least qualitatively) with our previous studies for the lithium ($^2S \rightarrow {}^2P$) [17], beryllium ($^1S \rightarrow {}^1P$) [15], and boron ($^2S \rightarrow {}^2P$) [18] atoms.

The agreement or lack thereof between the oscillator strengths calculated in this study and the available literature values reflects the accuracy of the methods used to generate the wave functions. The present work not only provides new benchmark values for the Be oscillator strengths but also extends the range of the considered $S-P$ transitions beyond what has been calculated in the previous studies. Additionally, our calculations of the transition dipole moments and the corresponding oscillator strengths are done with accounting for finite nuclear mass of beryllium. Although experimental measurements are not yet available for most of the considered transitions to thoroughly assess the accuracy of the present

TABLE IV. The absolute squares of the multiplet absorption transition dipole matrix elements, in the length ($|\boldsymbol{\mu}_{if}^{\mathrm{L}}|^2$) and velocity ($|\boldsymbol{\mu}_{if}^{\mathrm{V}}|^2$) formalisms for the transitions involving $^3S^e$ and $^3P^o$ states. The numbers in parentheses are estimated uncertainties due to the basis truncation.

Transition	$\lvert\boldsymbol{\mu}_{if}^{\mathrm{L}}\rvert^2$(^{9}Be)	$\lvert\boldsymbol{\mu}_{if}^{\mathrm{L}}\rvert^2$($^\infty$Be)	$\lvert\boldsymbol{\mu}_{if}^{\mathrm{V}}\rvert^2$(^{9}Be)	$\lvert\boldsymbol{\mu}_{if}^{\mathrm{V}}\rvert^2$($^\infty$Be)
$2\,^3P \to 3\,^3S$	8.083 114(38)	8.083 377(38)	$1.521\,120\,1(49) \times 10^{-1}$	$1.521\,080\,8(49) \times 10^{-1}$
MCHF [52,53]		8.31(83)		
$3\,^3S \to 3\,^3P$	$1.628\,845\,93(28) \times 10^{2}$	$1.628\,629\,67(28) \times 10^{2}$	$1.574\,942(16) \times 10^{-1}$	$1.575\,120(16) \times 10^{-1}$
MCHF [52,53]		$1.63(16) \times 10^{2}$		
$3\,^3S \to 4\,^3P$	$1.986\,413(37) \times 10^{-1}$	$1.989\,659(37) \times 10^{-1}$	$8.9462(10) \times 10^{-4}$	$8.9626(10) \times 10^{-4}$
MCHF [53]		$2.37(60) \times 10^{-1}$		
$3\,^3S \to 5\,^3P$	$4.0526(50) \times 10^{-4}$	$4.1402(50) \times 10^{-4}$	$2.7226(23) \times 10^{-6}$	$2.7774(23) \times 10^{-6}$
$3\,^3S \to 6\,^3P$	$1.939\,05(62) \times 10^{-3}$	$1.926\,07(62) \times 10^{-3}$	$1.5543(13) \times 10^{-5}$	$1.5446(13) \times 10^{-5}$
$3\,^3S \to 7\,^3P$	$2.933\,96(66) \times 10^{-3}$	$2.921\,88(66) \times 10^{-3}$	$2.5892(18) \times 10^{-5}$	$2.5794(18) \times 10^{-5}$
$3\,^3S \to 8\,^3P$	$2.735\,51(84) \times 10^{-3}$	$2.726\,30(84) \times 10^{-3}$	$2.5616(44) \times 10^{-5}$	$2.5540(44) \times 10^{-5}$
$3\,^3S \to 9\,^3P$	$2.262\,78(93) \times 10^{-3}$	$2.2545(93) \times 10^{-3}$	$2.195(13) \times 10^{-5}$	$2.189(13) \times 10^{-5}$
$3\,^3S \to 10\,^3P$	$1.834(42) \times 10^{-3}$	$1.828(42) \times 10^{-3}$	$1.816(53) \times 10^{-5}$	$1.808(53) \times 10^{-5}$
$3\,^3S \to 11\,^3P$	$1.5004(78) \times 10^{-3}$	$1.4957(78) \times 10^{-3}$	$1.533(19) \times 10^{-5}$	$1.529(19) \times 10^{-5}$
$2\,^3P \to 4\,^3S$	$8.0714(12) \times 10^{-1}$	$8.0709(12) \times 10^{-1}$	$3.031\,019(45) \times 10^{-2}$	$3.030\,790(45) \times 10^{-2}$
MCHF [53]		$8.1(20) \times 10^{-1}$		
$3\,^3P \to 4\,^3S$	$1.137\,459\,4(55) \times 10^{2}$	$1.137\,481\,7(55) \times 10^{2}$	$7.405\,053(60) \times 10^{-2}$	$7.405\,158(60) \times 10^{-2}$
MCHF [53]		$1.15(12) \times 10^{2}$		
$4\,^3S \to 4\,^3P$	$6.906\,627\,6(50) \times 10^{2}$	$6.905\,527\,3(50) \times 10^{2}$	$7.615\,82(11) \times 10^{-2}$	$7.616\,56(11) \times 10^{-2}$
$4\,^3S \to 5\,^3P$	2.383 80(12)	2.385 60(12)	$1.529\,079(86) \times 10^{-3}$	$1.530\,398(86) \times 10^{-3}$
MCHF [53]		2.58(65)		
$4\,^3S \to 6\,^3P$	$1.6915(11) \times 10^{-1}$	$1.6943(11) \times 10^{-1}$	$1.832\,38(35) \times 10^{-4}$	$1.835\,14(35) \times 10^{-4}$
MCHF [53]		$2.0(10) \times 10^{-1}$		
$4\,^3S \to 7\,^3P$	$2.6174(25) \times 10^{-2}$	$2.6246(25) \times 10^{-2}$	$3.6429(53) \times 10^{-5}$	$3.6513(53) \times 10^{-5}$
$4\,^3S \to 8\,^3P$	$5.7287(19) \times 10^{-3}$	$5.753(2) \times 10^{-3}$	$9.238(41) \times 10^{-6}$	$9.271(41) \times 10^{-6}$
$4\,^3S \to 9\,^3P$	$1.476(16) \times 10^{-3}$	$1.486(16) \times 10^{-3}$	$2.590(40) \times 10^{-6}$	$2.610(40) \times 10^{-6}$
$4\,^3S \to 10\,^3P$	$4.26(12) \times 10^{-4}$	$4.30(12) \times 10^{-4}$	$8.09(30) \times 10^{-7}$	$8.16(30) \times 10^{-7}$
$4\,^3S \to 11\,^3P$	$1.274(26) \times 10^{-4}$	$1.294(25) \times 10^{-4}$	$2.68(18) \times 10^{-7}$	$2.72(18) \times 10^{-7}$
$2\,^3P \to 5\,^3S$	$2.576\,11(41) \times 10^{-1}$	$2.575\,78(41) \times 10^{-1}$	$1.183\,220(28) \times 10^{-2}$	$1.183\,115(28) \times 10^{-2}$
MCHF [53]		$2.59(65) \times 10^{-1}$		
$3\,^3P \to 5\,^3S$	6.8275(19)	6.8267(19)	$1.446\,788(36) \times 10^{-2}$	$1.446\,715(36) \times 10^{-2}$
MCHF [53]		6.84(68)		
$4\,^3P \to 5\,^3S$	$4.603\,374(73) \times 10^{2}$	$4.603\,424(73) \times 10^{2}$	$4.620\,268(71) \times 10^{-2}$	$4.620\,377(71) \times 10^{-2}$
$5\,^3S \to 5\,^3P$	$1.918\,802\,5(36) \times 10^{3}$	$1.918\,480\,3(36) \times 10^{3}$	$4.43\,646(84) \times 10^{-2}$	$4.435\,013(84) \times 10^{-2}$
$5\,^3S \to 6\,^3P$	8.8396(17)	8.8448(17)	$1.357\,84(38) \times 10^{-3}$	$1.358\,62(38) \times 10^{-3}$
$5\,^3S \to 7\,^3P$	$8.6149(80) \times 10^{-1}$	$8.6241(80) \times 10^{-1}$	$2.4313(24) \times 10^{-4}$	$2.4332(24) \times 10^{-4}$
MCHF [53]		$9.6(24) \times 10^{-1}$		
$5\,^3S \to 8\,^3P$	$1.9192(45) \times 10^{-1}$	$1.9229(45) \times 10^{-1}$	$7.361(31) \times 10^{-5}$	$7.370(31) \times 10^{-5}$
$5\,^3S \to 9\,^3P$	$6.377(21) \times 10^{-2}$	$6.385(21) \times 10^{-2}$	$2.937(22) \times 10^{-5}$	$2.938(22) \times 10^{-5}$
$5\,^3S \to 10\,^3P$	$2.699(29) \times 10^{-2}$	$2.702(29) \times 10^{-2}$	$1.396(27) \times 10^{-5}$	$1.399(27) \times 10^{-2}$
$5\,^3S \to 11\,^3P$	$1.3508(59) \times 10^{-2}$	$1.3607(59) \times 10^{-2}$	$7.68(10) \times 10^{-6}$	$7.693(99) \times 10^{-6}$
$2\,^3P \to 6\,^3S$	$1.179\,86(37) \times 10^{-1}$	$1.179\,76(37) \times 10^{-}$	$5.925\,877(97) \times 10^{-3}$	$5.925\,196(97) \times 10^{-3}$
MCHF [53]		$1.19(30) \times 10^{-1}$		
$3\,^3P \to 6\,^3S$	1.9160(15)	1.9157(15)	$5.973\,68(17) \times 10^{-3}$	$5.973\,14(17) \times 10^{-3}$
MCHF [53]		1.92(19)		
$4\,^3P \to 6\,^3S$	$2.3315(14) \times 10^{1}$	$2.3312(14) \times 10^{1}$	$9.154\,43(57) \times 10^{-3}$	$9.153\,77(57) \times 10^{-3}$
MCHF [53]		$2.33(23) \times 10^{1}$		
$5\,^3P \to 6\,^3S$	$1.265\,800(27) \times 10^{3}$	$1.265\,803(27) \times 10^{3}$	$3.151\,308(76) \times 10^{-2}$	$3.151\,331(76) \times 10^{-2}$
$6\,^3S \to 6\,^3P$	$4.289\,562(45) \times 10^{3}$	$4.288\,854(45) \times 10^{3}$	$2.893\,42(24) \times 10^{-2}$	$2.893\,45(24) \times 10^{-2}$
$6\,^3S \to 7\,^3P$	$2.893\,45(24) \times 10^{1}$	$2.2584(12) \times 10^{1}$	$1.107\,14(47) \times 10^{-3}$	$1.107\,43(47) \times 10^{-3}$
$6\,^3S \to 8\,^3P$	2.4746(39)	2.4744(39)	$2.3751(26) \times 10^{-4}$	$2.3756(26) \times 10^{-4}$
$6\,^3S \to 9\,^3P$	$6.155(23) \times 10^{-1}$	$6.148(23) \times 10^{-1}$	$8.380(24) \times 10^{-5}$	$8.380(24) \times 10^{-5}$
$6\,^3S \to 10\,^3P$	$2.246(31) \times 10^{-1}$	$2.243(31) \times 10^{-1}$	$3.809(52) \times 10^{-5}$	$3.810(52) \times 10^{-5}$
$6\,^3S \to 11\,^3P$	$1.0405(99) \times 10^{-1}$	$1.0390(99) \times 10^{-1}$	$2.042(18) \times 10^{-5}$	$2.043(18) \times 10^{-5}$

TABLE IV. (*Continued*.)

Transition	$\lvert\boldsymbol{\mu}^{\mathrm{L}}_{if}\rvert^2(^9\mathrm{Be})$	$\lvert\boldsymbol{\mu}^{\mathrm{L}}_{if}\rvert^2(^\infty\mathrm{Be})$	$\lvert\boldsymbol{\mu}^{\mathrm{V}}_{if}\rvert^2(^9\mathrm{Be})$	$\lvert\boldsymbol{\mu}^{\mathrm{V}}_{if}\rvert^2(^\infty\mathrm{Be})$
$2\,^3P \rightarrow 7\,^3S$	$6.4665(13) \times 10^{-2}$	$6.4652(13) \times 10^{-2}$	$3.407\,71(26) \times 10^{-3}$	$3.407\,31(26) \times 10^{-3}$
MCHF [53]		$6.5(16) \times 10^{-2}$		
$3\,^3P \rightarrow 7\,^3S$	$8.3854(48) \times 10^{-1}$	$8.3835(48) \times 10^{-1}$	$3.148\,14(20) \times 10^{-3}$	$3.147\,63(20) \times 10^{-3}$
MCHF [53]		$8.37(84) \times 10^{-1}$		
$4\,^3P \rightarrow 7\,^3S$	6.132(12)	6.130(12)	$3.911\,97(31) \times 10^{-3}$	$3.911\,57(31) \times 10^{-1}$
MCHF [53]		6.12(61)		
$5\,^3P \rightarrow 7\,^3S$	$5.8260(25) \times 10^{1}$	$5.8250(25) \times 10^{1}$	$6.340\,23(24) \times 10^{-3}$	$6.339\,72(24) \times 10^{-3}$
$6\,^3P \rightarrow 7\,^3S$	$2.816\,59(20) \times 10^{3}$	$2.816\,59(20) \times 10^{3}$	$2.281\,34(11) \times 10^{-2}$	$2.281\,39(11) \times 10^{-2}$
$7\,^3S \rightarrow 7\,^3P$	$8.352\,77(53) \times 10^{3}$	$8.351\,55(53) \times 10^{3}$	$2.034\,35(26) \times 10^{-2}$	$2.034\,23(26) \times 10^{-2}$
$7\,^3S \rightarrow 8\,^3P$	$4.7435(46) \times 10^{1}$	$4.7469(46) \times 10^{1}$	$8.9599(64) \times 10^{-4}$	$8.9582(64) \times 10^{-4}$
$7\,^3S \rightarrow 9\,^3P$	5.528(29)	5.520(29)	$2.1409(72) \times 10^{-4}$	$2.1396(72) \times 10^{-4}$
$7\,^3S \rightarrow 10\,^3P$	1.455(31)	1.450(31)	$8.206(99) \times 10^{-5}$	$8.198(99) \times 10^{-5}$
$7\,^3S \rightarrow 11\,^3P$	$5.50(13) \times 10^{-1}$	$5.49(13) \times 10^{-1}$	$4.008(49) \times 10^{-5}$	$4.011(49) \times 10^{-5}$
$2\,^3P \rightarrow 8\,^3S$	$3.9534(8) \times 10^{-2}$	$3.952\,02(83) \times 10^{-2}$	$2.144\,19(11) \times 10^{-3}$	$2.143\,67(11) \times 10^{-3}$
MCHF [53]		$4.0(10) \times 10^{-2}$		
$3\,^3P \rightarrow 8\,^3S$	$4.5235(14) \times 10^{-1}$	$4.5217(14) \times 10^{-1}$	$1.888\,15(21) \times 10^{-3}$	$1.887\,55(21) \times 10^{-3}$
MCHF [53]		$4.51(45) \times 10^{-1}$		
$4^3P \rightarrow 8^3S$	2.6021(11)	2.6011(11)	$2.127\,40(41) \times 10^{-3}$	$2.126\,73(41) \times 10^{-3}$
MCHF [53]		2.59(26)		
$5^3P \rightarrow 8^3S$	$1.4638(20) \times 10^{1}$	$1.4632(20) \times 10^{1}$	$2.777\,56(99) \times 10^{-3}$	$2.776\,79(99) \times 10^{-3}$
$6^3P \rightarrow 8^3S$	$1.2148(25) \times 10^{2}$	$1.2148(25) \times 10^{2}$	$4.648\,15(64) \times 10^{-3}$	$4.646\,62(64) \times 10^{-3}$
$7^3P \rightarrow 8^3S$	$5.4687(18) \times 10^{3}$	$5.4689(18) \times 10^{3}$	$1.725\,48(17) \times 10^{-2}$	$1.725\,22(17) \times 10^{-2}$
$8^3S \rightarrow 3^3P$	$1.476\,56(41) \times 10^{4}$	$1.476\,38(41) \times 10^{4}$	$1.507\,10(36) \times 10^{-2}$	$1.506\,73(36) \times 10^{-2}$
$8^3S \rightarrow 9^3P$	$8.799(96) \times 10^{1}$	$8.790(96) \times 10^{1}$	$7.316(37) \times 10^{-4}$	$7.307(37) \times 10^{-4}$
$8^3S \rightarrow 10^3P$	$1.079(63) \times 10^{1}$	$1.075(63) \times 10^{1}$	$1.892(39) \times 10^{-4}$	$1.889(39) \times 10^{-4}$
$8^3S \rightarrow 11^3P$	2.93(14)	2.92(14)	$7.65(15) \times 10^{-5}$	$7.65(15) \times 10^{-5}$
$2^3P \rightarrow 9^3S$	$2.603\,01(47) \times 10^{-2}$	$2.601\,48(47) \times 10^{-2}$	$1.438\,48(34) \times 10^{-3}$	$1.437\,63(17) \times 10^{-3}$
$3^3P \rightarrow 9^3S$	$2.7561(8) \times 10^{-1}$	$2.7544(8) \times 10^{-1}$	$1.229\,68(17) \times 10^{-3}$	$1.228\,98(34) \times 10^{-3}$
$4^3P \rightarrow 9^3S$	1.382 84(95)	1.382 01(95)	$1.310\,82(42) \times 10^{-3}$	$1.310\,08(42) \times 10^{-3}$
$5^3P \rightarrow 9^3S$	6.074(11)	6.070(11)	$1.546\,23(52) \times 10^{-3}$	$1.545\,34(52) \times 10^{-3}$
$6^3P \rightarrow 9^3S$	$2.9561(96) \times 10^{1}$	$2.9545(96) \times 10^{1}$	$2.0743(11) \times 10^{-3}$	$2.0738(11) \times 10^{-3}$
$7^3P \rightarrow 9^3S$	$2.255(18) \times 10^{2}$	$2.255(18) \times 10^{2}$	$3.5487(39) \times 10^{-3}$	$3.5463(39) \times 10^{-3}$
$8^3P \rightarrow 9^3S$	$9.6466(97) \times 10^{2}$	$9.6480(97) \times 10^{2}$	$1.349\,10(39) \times 10^{-2}$	$1.348\,65(39) \times 10^{-2}$
$9^3S \rightarrow 4^3P$	$2.4263(41) \times 10^{4}$	$2.4263(41) \times 10^{4}$	$1.1620(18) \times 10^{-2}$	$1.1615(18) \times 10^{-2}$
$9^3S \rightarrow 10^3P$	$1.47(16) \times 10^{2}$	$1.46(16) \times 10^{2}$	$6.05(24) \times 10^{-4}$	$6.04(24) \times 10^{-4}$
$9^3S \rightarrow 11^3P$	$1.919(46) \times 10^{1}$	$1.910(46) \times 10^{1}$	$1.675(27) \times 10^{-4}$	$1.669(27) \times 10^{-4}$
$2^3P \rightarrow 10^3S$	$1.809\,55(32) \times 10^{-2}$	$1.808\,01(32) \times 10^{-2}$	$1.012\,88(24) \times 10^{-3}$	$1.012\,1(2) \times 10^{-3}$
$3^3P \rightarrow 10^3S$	$1.8193(12) \times 10^{-1}$	$1.8178(12) \times 10^{-1}$	$8.4916(36) \times 10^{-4}$	$8.485(4) \times 10^{-4}$
$4^3P \rightarrow 10^3S$	$8.372(12) \times 10^{-1}$	$8.366(12) \times 10^{-1}$	$8.7374(48) \times 10^{-4}$	$8.731(5) \times 10^{-4}$
$5^3P \rightarrow 10^3S$	3.1860(94)	3.1840(94)	$9.7268(41) \times 10^{-4}$	$9.719(4) \times 10^{-4}$
$6^3P \rightarrow 10^3S$	$1.2052(59) \times 10^{1}$	$1.2039(59) \times 10^{1}$	$1.1749(12) \times 10^{-3}$	$1.1739(12) \times 10^{-3}$
$7^3P \rightarrow 10^3S$	$5.345(76) \times 10^{1}$	$5.340(76) \times 10^{1}$	$1.6082(23) \times 10^{-3}$	$1.6065(23) \times 10^{-3}$
$8^3P \rightarrow 10^3S$	$3.831(46) \times 10^{2}$	$3.832(46) \times 10^{2}$	$2.8014(84) \times 10^{-3}$	$2.7982(84) \times 10^{-3}$
$9^3P \rightarrow 10^3S$	$1.5553(34) \times 10^{3}$	$1.5555(34) \times 10^{3}$	$1.0836(20) \times 10^{-2}$	$1.0829(20) \times 10^{-2}$
$10^3S \rightarrow 5^3P$	$3.794(30) \times 10^{4}$	$3.797(30) \times 10^{4}$	$9.209(24) \times 10^{-3}$	$9.196(24) \times 10^{-3}$
$10^3S \rightarrow 11^3P$	$2.437(24) \times 10^{2}$	$2.437(24) \times 10^{2}$	$5.203(39) \times 10^{-4}$	$5.189(39) \times 10^{-4}$
$2^3P \rightarrow 11^3S$	$1.3135(11) \times 10^{-2}$	$1.3119(11) \times 10^{-2}$	$7.423(65) \times 10^{-4}$	$7.415(7) \times 10^{-4}$
$3^3P \rightarrow 11^3S$	$1.2749(11) \times 10^{-1}$	$1.2735(11) \times 10^{-1}$	$6.1406(48) \times 10^{-4}$	$6.134(5) \times 10^{-4}$
$4^3P \rightarrow 11^3S$	$5.5532(49) \times 10^{-1}$	$5.5525(49) \times 10^{-1}$	$6.1694(42) \times 10^{-4}$	$6.162(4) \times 10^{-4}$
$5^3P \rightarrow 11^3S$	1.9232(43)	1.9214(43)	$6.6202(95) \times 10^{-4}$	$6.613(9) \times 10^{-4}$
$6^3P \rightarrow 11^3S$	6.255(51)	6.250(51)	$7.5274(63) \times 10^{-4}$	$7.520(6) \times 10^{-4}$
$7^3P \rightarrow 11^3S$	$2.132(15) \times 10^{1}$	$2.128(15) \times 10^{1}$	$9.249(21) \times 10^{-4}$	$9.237(21) \times 10^{-4}$
$8^3P \rightarrow 11^3S$	$8.96(17) \times 10^{1}$	$8.95(17) \times 10^{1}$	$1.2843(72) \times 10^{-3}$	$1.2824(72) \times 10^{-3}$
$9^3P \rightarrow 11^3S$	$6.09(26) \times 10^{2}$	$6.07(26) \times 10^{2}$	$2.271(28) \times 10^{-3}$	$2.268(28) \times 10^{-3}$
$10^3P \rightarrow 11^3S$	$2.45(15) \times 10^{3}$	$2.45(15) \times 10^{3}$	$8.90(21) \times 10^{-3}$	$8.84(21) \times 10^{-3}$
$11^3S \rightarrow 6^3P$	$5.57(11) \times 10^{4}$	$5.57(11) \times 10^{4}$	$7.61(20) \times 10^{-3}$	$7.61(20) \times 10^{-3}$

TABLE IV. (*Continued.*)

Transition	$\lvert\boldsymbol{\mu}^{\mathrm{L}}_{if}\rvert^2$(^{9}Be)	$\lvert\boldsymbol{\mu}^{\mathrm{L}}_{if}\rvert^2$($^\infty$Be)	$\lvert\boldsymbol{\mu}^{\mathrm{V}}_{if}\rvert^2$(^{9}Be)	$\lvert\boldsymbol{\mu}^{\mathrm{V}}_{if}\rvert^2$($^\infty$Be)
$2^3P \to 12^3S$	$9.887(73) \times 10^{-3}$	$9.88(7) \times 10^{-3}$	$5.630(48) \times 10^{-4}$	$5.627(48) \times 10^{-4}$
$3^3P \to 12^3S$	$9.337(55) \times 10^{-2}$	$9.322(55) \times 10^{-2}$	$4.601(26) \times 10^{-4}$	$4.597(26) \times 10^{-4}$
$4^3P \to 12^3S$	$3.886(27) \times 10^{-1}$	$3.881(27) \times 10^{-1}$	$4.550(31) \times 10^{-4}$	$4.545(31) \times 10^{-4}$
$5^3P \to 12^3S$	1.2657(84)	1.264(8)	$4.754(32) \times 10^{-4}$	$4.750(32) \times 10^{-4}$
$6^3P \to 12^3S$	3.733(45)	3.728(45)	$5.202(34) \times 10^{-4}$	$5.197(34) \times 10^{-4}$
$7^3P \to 12^3S$	$1.0920(66) \times 10^{1}$	$1.090(7) \times 10^{1}$	$6.023(44) \times 10^{-4}$	$6.017(44) \times 10^{-4}$
$8^3P \to 12^3S$	$3.534(19) \times 10^{1}$	$3.528(19) \times 10^{1}$	$7.522(34) \times 10^{-4}$	$7.508(34) \times 10^{-4}$
$9^3P \to 12^3S$	$1.438(81) \times 10^{2}$	$1.436(81) \times 10^{2}$	$1.0578(97) \times 10^{-3}$	$1.0557(97) \times 10^{-3}$
$10^3P \to 12^3S$	$9.8(17) \times 10^{2}$	$9.8(17) \times 10^{2}$	$1.91(11) \times 10^{-3}$	$1.89(11) \times 10^{-3}$
$11^3P \to 12^3S$	$3.65(11) \times 10^{4}$	$3.65(11) \times 10^{4}$	$7.441(67) \times 10^{-3}$	$7.434(67) \times 10^{-3}$

results, future advancements may make such an assessment possible.

It is noteworthy that this study provides a highly accurate treatment of oscillator strengths for $S-P$ transitions involving highly excited triplet states of Be up to principal quantum numbers $n_S \leqslant 12$ and $n_P \leqslant 11$. States beyond this range, however, remain uncharacterized. To address this, we estimate the oscillator strengths of higher-lying Rydberg states by adapting the analytical expression for transition dipole matrix elements ($|n_1, l\rangle \to |n_2, l+1\rangle$) in a hydrogen-like atom (see Condon and Shortley [58]), augmented with fitting parameters similar to quantum-defect corrections. Because the exact expression for dipole matrix elements exhibits complex behavior that depends strongly on the asymptotic path chosen, no single asymptotic formula provides a satisfactory description in the two-dimensional case (arbitrarily large n_S and n_P). However, a particularly useful special case arises when $n_S = n_P$, i.e., for transitions between states with the same principal quantum number. In this situation, for a hydrogen-like atom the transition dipole matrix elements simplify to [58]

$$\left|\boldsymbol{\mu}^{\mathrm{L}}_{if}\right|^2 = \left(\tfrac{3}{2} n\sqrt{n^2 - l^2}\right)^2. \tag{11}$$

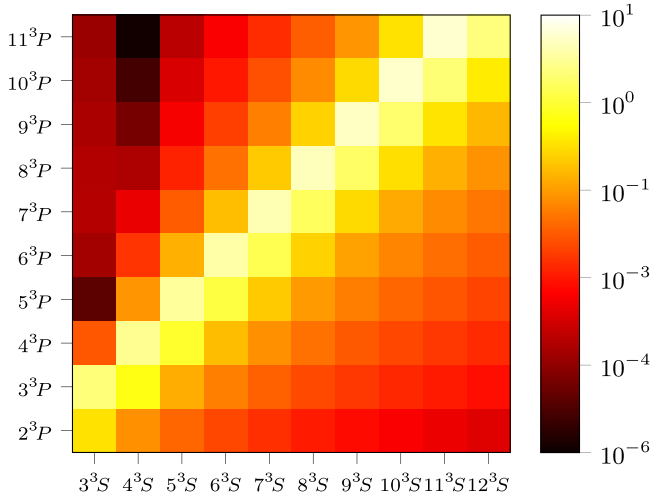

FIG. 2. Heatmap plot of absorption oscillator strengths (^{9}Be isotope, length guage) for the triplet state transitions considered in this work.

In the limit $n \to \infty$, this expression scales as $|\boldsymbol{\mu}^{\mathrm{L}}_{if}|^2 \approx n^4$. Since the transition energy ΔE_{if} entering the oscillator strength is proportional to $1/n^3$ for large n, the corresponding oscillator strength scales linearly with n. To examine how well the beryllium oscillator strength data obtained in this work follow this trend, we extracted the values along the diagonal $n_S = n_P$ from Fig. 2 and plotted them as a function of n in Fig. 3. Extrapolation of these data yields a slope parameter $a = 0.4148(10)$ in the linear relation $f = a\,n$. We believe this value allows one to predict oscillator strengths for $n > 11$ with an accuracy of about three significant figures, or slightly less.

IV. SUMMARY

In this study, transitions between the $n\,^3P$ ($n = 2-11$) and $n\,^3S$ ($n = 3-12$) states of the beryllium atom are investigated. Using the Rayleigh-Ritz variational method and expanding the wave functions with all-particle explicitly correlated Gaussian basis functions, we perform highly accurate nonrelativistic calculations to determine the total energies and corresponding wave functions of the states. Using these results, the absorption transition energies and oscillator strengths are computed for all $^3P \to {}^3S$ and $^3S \to {}^3P$ transitions between the considered states for both ^{9}Be and $^\infty$Be.

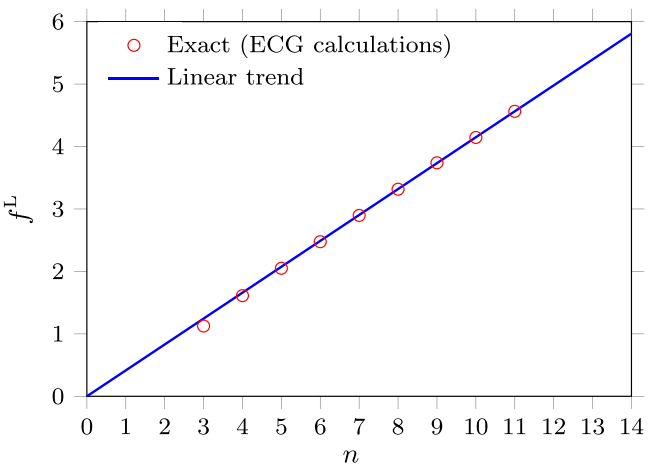

FIG. 3. Absorption oscillator strengths for the ($n\,^3S \to n\,^2P, n = 3-11$) triplet state transitions in beryllium.

TABLE V. Nonrelativistic multiplet absorption oscillator strengths obtained using the length (f_{if}^{L}) and velocity (f_{if}^{V}) formalisms for the transitions involving $^3S^e$ and $^3P^o$ states of the beryllium atom. The uncertainties (shown in parentheses) are calculated as the root mean squares of the uncertainties of $|\boldsymbol{\mu}_{if}^{\mathrm{L}}|^2$ or $|\boldsymbol{\mu}_{if}^{\mathrm{V}}|^2$ and ΔE, where ΔE is the difference between the nonrelativistic total energies of the initial (i) and final (f) states.

Transition	$f_{if}^{\mathrm{L}}(^9\mathrm{Be})$	$f_{if}^{\mathrm{V}}(^9\mathrm{Be})$	$f_{if}^{\mathrm{L}}(^\infty\mathrm{Be})$	$f_{if}^{\mathrm{V}}(^\infty\mathrm{Be})$
$2^3P \rightarrow 3^3S$	$8.213\,671(39) \times 10^{-2}$	$8.213\,673(27) \times 10^{-2}$	$8.213\,700(39) \times 10^{-2}$	$8.213\,698(27) \times 10^{-2}$
MCHF [52,53]			$8.44(84) \times 10^{-2}$	
BCICP [46]			8.23×10^{-2}	
TDGI [47,48]			2.63×10^{-2}	2.56×10^{-2}
$3^3S \rightarrow 3^3P$	1.125 537 00(41)	1.125 537(42)	1.125 528 03(41)	1.125 524(11)
MCHF [52,53]			1.13(11)	
BCICP [46]			1.126	
$3^3S \rightarrow 4^3P$	$2.962\,450(55) \times 10^{-3}$	$2.962\,32(33) \times 10^{-3}$	$2.967\,521(55) \times 10^{-3}$	$2.967\,52(33) \times 10^{-3}$
MCHF [53]			$3.53(88) \times 10^{-3}$	
BCICP [46]			3.01×10^{-3}	
$3^3S \rightarrow 5^3P$	$7.379(9) \times 10^{-6}$	$7.384(6) \times 10^{-6}$	$7.539(9) \times 10^{-6}$	$7.532(6) \times 10^{-6}$
BCICP [46]			9×10^{-6}	
$3^3S \rightarrow 6^3P$	$3.8576(12) \times 10^{-5}$	$3.8581(33) \times 10^{-5}$	$3.8320(12) \times 10^{-5}$	$3.8339(33) \times 10^{-5}$
BCICP [46]			3.6×10^{-5}	
$3^3S \rightarrow 7^3P$	$6.1242(14) \times 10^{-5}$	$6.1255(44) \times 10^{-5}$	$6.0994(14) \times 10^{-5}$	$6.1019(44) \times 10^{-5}$
BCICP [46]			5.9×10^{-5}	
$3^3S \rightarrow 8^3P$	$5.8793(29) \times 10^{-5}$	$5.886(16) \times 10^{-5}$	$5.8599(29) \times 10^{-5}$	$5.868(16) \times 10^{-5}$
BCICP [46]			5.7×10^{-5}	
$3^3S \rightarrow 9^3P$	$4.958(20) \times 10^{-5}$	$4.947(30) \times 10^{-5}$	$4.940(20) \times 10^{-5}$	$4.933(30) \times 10^{-5}$
$3^3S \rightarrow 10^3P$	$4.073(93) \times 10^{-5}$	$4.04(12) \times 10^{-5}$	$4.059(93) \times 10^{-5}$	$4.02(12) \times 10^{-5}$
$3^3S \rightarrow 11^3P$	$3.364(18) \times 10^{-5}$	$3.376(42) \times 10^{-5}$	$3.353(18) \times 10^{-5}$	$3.368(42) \times 10^{-5}$
$2^3P \rightarrow 4^3S$	$1.158\,64(18) \times 10^{-2}$	$1.158\,569(17) \times 10^{-2}$	$1.158\,56(18) \times 10^{-2}$	$1.158\,483(17) \times 10^{-2}$
MCHF [53]			$1.17(29) \times 10^{-2}$	
$3^3P \rightarrow 4^3S$	$2.149\,801(10) \times 10^{-1}$	$2.149\,802(18) \times 10^{-1}$	$2.149\,837(10) \times 10^{-1}$	$2.149\,838(18) \times 10^{-1}$
MCHF [53]			$2.18(22) \times 10^{-1}$	
BCICP [46]			2.15×10^{-1}	
$4^3S \rightarrow 3^3P$	1.611 683 4(53)	1.611 677(23)	1.611 640 4(53)	1.611 619(23)
BCICP [46]			1.612	
$4^3S \rightarrow 5^3P$	$1.341\,641(69) \times 10^{-2}$	$1.341\,648(75) \times 10^{-2}$	$1.342\,760(69) \times 10^{-2}$	$1.342\,698(75) \times 10^{-2}$
MCHF [53]			$1.45(36) \times 10^{-2}$	
BCICP [46]			1.35×10^{-2}	
$4^3S \rightarrow 6^3P$	$1.2372(12) \times 10^{-3}$	$1.237\,17(28) \times 10^{-3}$	$1.2393(12) \times 10^{-3}$	$1.238\,94(47) \times 10^{-3}$
MCHF [53]			$1.5(8) \times 10^{-3}$	
BCICP [46]			1.26×10^{-3}	
$4^3S \rightarrow 7^3P$	$2.1707(21) \times 10^{-4}$	$2.1692(32) \times 10^{-4}$	$2.1768(21) \times 10^{-4}$	$2.1740(32) \times 10^{-4}$
BCICP [46]			2.23×10^{-4}	
$4^3S \rightarrow 8^3P$	$5.1057(17) \times 10^{-5}$	$5.119(23) \times 10^{-5}$	$5.1281(17) \times 10^{-5}$	$5.137(23) \times 10^{-5}$
BCICP [46]			5.31×10^{-5}	
$4^3S \rightarrow 9^3P$	$1.377(15) \times 10^{-5}$	$1.371(21) \times 10^{-5}$	$1.387(15) \times 10^{-5}$	$1.382(21) \times 10^{-5}$
$4^3S \rightarrow 10^3P$	$4.10(11) \times 10^{-6}$	$4.15(22) \times 10^{-6}$	$4.14(11) \times 10^{-6}$	$4.19(22) \times 10^{-6}$
$4^3S \rightarrow 11^3P$	$1.253(25) \times 10^{-6}$	$1.346(91) \times 10^{-6}$	$1.273(25) \times 10^{-6}$	$1.365(91) \times 10^{-6}$
$2^3P \rightarrow 5^3S$	$4.089\,53(66) \times 10^{-3}$	$4.089\,681(96) \times 10^{-3}$	$4.089\,03(66) \times 10^{-3}$	$4.089\,293(96) \times 10^{-3}$
MCHF [53]			$4.1(10) \times 10^{-3}$	
BCICP [46]			4.10×10^{-3}	
$3^3P \rightarrow 5^3S$	$2.328\,13(64) \times 10^{-2}$	$2.328\,035(58) \times 10^{-2}$	$2.327\,94(64) \times 10^{-2}$	$2.327\,851(58) \times 10^{-2}$
MCHF [53]			$2.33(23) \times 10^{-2}$	
BCICP [46]			2.33×10^{-2}	
$4^3P \rightarrow 5^3S$	$3.416\,177(55) \times 10^{-1}$	$3.416\,139(53) \times 10^{-1}$	$3.416\,210(55) \times 10^{-1}$	$3.416\,224(53) \times 10^{-1}$
BCICP [46]			3.418×10^{-1}	
$5^3S \rightarrow 5^3P$	2.049 890(26)	2.049 905(39)	2.049 825(26)	2.049 795(39)
BCICP [46]			2.051	
$5^3S \rightarrow 6^3P$	$2.434\,64(46) \times 10^{-2}$	$2.434\,57(68) \times 10^{-2}$	$2.436\,27(46) \times 10^{-2}$	$2.435\,76(68) \times 10^{-2}$
BCICP [46]			2.45×10^{-2}	
$5^3S \rightarrow 7^3P$	$3.2164(30) \times 10^{-3}$	$3.2158(32) \times 10^{-3}$	$3.2200(30) \times 10^{-3}$	$3.2182(32) \times 10^{-3}$

TABLE V. (*Continued.*)

Transition	$f_{if}^{\mathrm{L}}(^9\mathrm{Be})$	$f_{if}^{\mathrm{V}}(^9\mathrm{Be})$	$f_{if}^{\mathrm{L}}(^\infty\mathrm{Be})$	$f_{if}^{\mathrm{V}}(^\infty\mathrm{Be})$
MCHF [53]			$3.58(90) \times 10^{-3}$	
BCICP [46]			3.25×10^{-3}	
$5^3S \to 8^3P$	$8.354(20) \times 10^{-4}$	$8.351(35) \times 10^{-4}$	$8.371(20) \times 10^{-4}$	$8.361(35) \times 10^{-4}$
BCICP [46]			8.47×10^{-4}	
$5^3S \to 9^3P$	$3.0415(99) \times 10^{-4}$	$3.041(22) \times 10^{-4}$	$3.0452(99) \times 10^{-4}$	$3.042(22) \times 10^{-4}$
$5^3S \to 10^3P$	$1.367(15) \times 10^{-4}$	$1.362(29) \times 10^{-4}$	$1.368(15) \times 10^{-4}$	$1.364(29) \times 10^{-4}$
$5^3S \to 11^3P$	$7.130(31) \times 10^{-5}$	$7.186(94) \times 10^{-5}$	$7.183(31) \times 10^{-5}$	$7.196(94) \times 10^{-5}$
$2^3P \to 6^3S$	$1.958\,63(62) \times 10^{-3}$	$1.958\,680(32) \times 10^{-3}$	$1.958\,48(62) \times 10^{-3}$	$1.958\,439(32) \times 10^{-3}$
MCHF [53]			$1.97(50) \times 10^{-3}$	
BCICP [46]			1.96×10^{-3}	
$3^3P \to 6^3S$	$7.9239(62) \times 10^{-3}$	$7.925\,56(23) \times 10^{-3}$	$7.9227(62) \times 10^{-3}$	$7.924\,57(23) \times 10^{-3}$
MCHF [53]			$7.92(80) \times 10^{-3}$	
BCICP [46]			7.92×10^{-3}	
$4^3P \to 6^3S$	$3.4222(21) \times 10^{-2}$	$3.422\,11(21) \times 10^{-2}$	$3.4218(21) \times 10^{-2}$	$3.421\,76(21) \times 10^{-2}$
MCHF [53]			$3.42(34) \times 10^{-2}$	
BCICP [46]			3.42×10^{-2}	
$5^3P \to 6^3S$	$4.678\,39(11) \times 10^{-1}$	$4.678\,34(11) \times 10^{-1}$	$4.678\,40(11) \times 10^{-1}$	$4.678\,38(11) \times 10^{-1}$
BCICP [46]			4.68×10^{-1}	
$6^3S \to 3^3P$	2.475 616(64)	2.475 81(27)	2.475 549(64)	2.475 49(27)
BCICP [46]			2.476	
$6^3S \to 7^3P$	$3.5119(18) \times 10^{-2}$	$3.5129(15) \times 10^{-2}$	$3.5152(18) \times 10^{-2}$	$3.5135(15) \times 10^{-2}$
BCICP [46]			3.54×10^{-2}	
$6^3S \to 8^3P$	$5.3839(85) \times 10^{-3}$	$5.3911(59) \times 10^{-3}$	$5.3838(85) \times 10^{-3}$	$5.3919(59) \times 10^{-3}$
BCICP [46]			5.45×10^{-3}	
$6^3S \to 9^3P$	$1.5956(59) \times 10^{-3}$	$1.5964(47) \times 10^{-3}$	$1.5938(59) \times 10^{-3}$	$1.5962(47) \times 10^{-3}$
$6^3S \to 10^3P$	$6.483(90) \times 10^{-4}$	$6.517(96) \times 10^{-4}$	$6.473(90) \times 10^{-4}$	$6.519(96) \times 10^{-4}$
$6^3S \to 11^3P$	$3.227(31) \times 10^{-4}$	$3.250(28) \times 10^{-4}$	$3.223(31) \times 10^{-4}$	$3.253(28) \times 10^{-4}$
$2^3P \to 7^3S$	$1.099\,54(22) \times 10^{-3}$	$1.099\,644(84) \times 10^{-3}$	$1.099\,33(22) \times 10^{-3}$	$1.099\,504(84) \times 10^{-3}$
MCHF [53]			$1.10(30) \times 10^{-3}$	
$3^3P \to 7^3S$	$3.8060(22) \times 10^{-3}$	$3.805\,76(24) \times 10^{-3}$	$3.8053(22) \times 10^{-3}$	$3.805\,00(24) \times 10^{-3}$
MCHF [53]			$3.80(40) \times 10^{-3}$	
$4^3P \to 7^3S$	$1.1473(23) \times 10^{-2}$	$1.147\,238(90) \times 10^{-2}$	$1.1470(23) \times 10^{-2}$	$1.147\,076(90) \times 10^{-2}$
MCHF [53]			$1.14(11) \times 10^{-2}$	
$5^3P \to 7^3S$	$4.5023(19) \times 10^{-2}$	$4.501\,67(17) \times 10^{-2}$	$4.5017(19) \times 10^{-2}$	$4.501\,16(17) \times 10^{-2}$
$6^3P \to 7^3S$	$5.937\,80(49) \times 10^{-1}$	$5.937\,75(27) \times 10^{-1}$	$5.937\,79(49) \times 10^{-1}$	$5.937\,86(27) \times 10^{-1}$
$7^3S \to 7^3P$	2.896 65(35)	2.896 91(37)	2.896 63(35)	2.896 33(37)
$7^3S \to 8^3P$	$4.5822(45) \times 10^{-2}$	$4.5804(33) \times 10^{-2}$	$4.5859(77) \times 10^{-2}$	$4.5791(55) \times 10^{-2}$
$7^3S \to 9^3P$	$7.643(40) \times 10^{-3}$	$7.646(26) \times 10^{-3}$	$7.632(40) \times 10^{-3}$	$7.641(26) \times 10^{-3}$
$7^3S \to 10^3P$	$2.440(53) \times 10^{-3}$	$2.417(31) \times 10^{-3}$	$2.431(53) \times 10^{-3}$	$2.415(31) \times 10^{-3}$
$7^3S \to 11^3P$	$1.040(24) \times 10^{-3}$	$1.046(13) \times 10^{-3}$	$1.039(24) \times 10^{-3}$	$1.047(13) \times 10^{-3}$
$2^3P \to 8^3S$	$6.8200(14) \times 10^{-4}$	$6.819\,99(37) \times 10^{-4}$	$6.8177(14) \times 10^{-4}$	$6.818\,28(37) \times 10^{-4}$
MCHF [53]			$6.8(20) \times 10^{-4}$	
$3^3P \to 8^3S$	$2.164\,94(65) \times 10^{-3}$	$2.164\,68(25) \times 10^{-3}$	$2.164\,18(65) \times 10^{-3}$	$2.163\,91(25) \times 10^{-3}$
MCHF [53]			$2.16(20) \times 10^{-3}$	
$4^3P \to 8^3S$	$5.5116(23) \times 10^{-3}$	$5.5109(11) \times 10^{-3}$	$5.5098(23) \times 10^{-3}$	$5.5089(11) \times 10^{-3}$
MCHF [53]			$5.49(55) \times 10^{-3}$	
$5^3P \to 8^3S$	$1.4930(20) \times 10^{-2}$	$1.494\,22(54) \times 10^{-2}$	$1.4925(20) \times 10^{-2}$	$1.493\,74(54) \times 10^{-2}$
$6^3P \to 8^3S$	$5.563(11) \times 10^{-2}$	$5.568\,93(77) \times 10^{-2}$	$5.564(11) \times 10^{-2}$	$5.566\,90(77) \times 10^{-2}$
$7^3P \to 8^3S$	$7.1946(35) \times 10^{-1}$	$7.196\,48(70) \times 10^{-1}$	$7.1948(35) \times 10^{-1}$	$7.195\,40(70) \times 10^{-1}$
$8^3S \to 3^3P$	3.3161(22)	3.313 93(78)	3.3161(22)	3.3126(13)
$8^3S \to 9^3P$	$5.641(62) \times 10^{-2}$	$5.636(29) \times 10^{-2}$	$5.635(62) \times 10^{-2}$	$5.629(29) \times 10^{-2}$
$8^3S \to 10^3P$	$1.009(59) \times 10^{-2}$	$9.99(21) \times 10^{-3}$	$1.005(59) \times 10^{-2}$	$9.97(21) \times 10^{-3}$
$8^3S \to 11^3P$	$3.38(16) \times 10^{-3}$	$3.284(64) \times 10^{-3}$	$3.36(16) \times 10^{-3}$	$3.284(64) \times 10^{-3}$
$2^3P \to 9^3S$	$4.532\,72(83) \times 10^{-4}$	$4.532\,66(60) \times 10^{-4}$	$4.530\,10(83) \times 10^{-4}$	$4.529\,94(60) \times 10^{-4}$
$3^3P \to 9^3S$	$1.363\,83(40) \times 10^{-3}$	$1.363\,50(38) \times 10^{-3}$	$1.363\,04(40) \times 10^{-3}$	$1.362\,67(38) \times 10^{-3}$
$4^3P \to 9^3S$	$3.1837(13) \times 10^{-3}$	$3.1537(10) \times 10^{-3}$	$3.1520(22) \times 10^{-3}$	$3.1518(10) \times 10^{-3}$
$5^3P \to 9^3S$	$7.152(22) \times 10^{-3}$	$7.1754(25) \times 10^{-3}$	$7.178(13) \times 10^{-3}$	$7.1710(25) \times 10^{-3}$
$6^3P \to 9^3S$	$1.8340(59) \times 10^{-2}$	$1.834\,54(97) \times 10^{-2}$	$1.8330(59) \times 10^{-2}$	$1.834\,01(97) \times 10^{-2}$

TABLE V. (*Continued*.)

Transition	$f_{if}^{\mathrm{L}}(^9\mathrm{Be})$	$f_{if}^{\mathrm{V}}(^9\mathrm{Be})$	$f_{if}^{\mathrm{L}}(^\infty\mathrm{Be})$	$f_{if}^{\mathrm{V}}(^\infty\mathrm{Be})$
$7^3P \rightarrow 9^3S$	$6.629(52) \times 10^{-2}$	$6.6234(73) \times 10^{-2}$	$6.630(52) \times 10^{-2}$	$6.6187(73) \times 10^{-2}$
$8^3P \rightarrow 9^3S$	$8.446(16) \times 10^{-1}$	$8.4546(24) \times 10^{-1}$	$8.447(27) \times 10^{-1}$	$8.4518(42) \times 10^{-1}$
$9^3S \rightarrow 4^3P$	3.739(13)	3.7236(58)	3.739(13)	3.7217(58)
$9^3S \rightarrow 10^3P$	$6.56(72) \times 10^{-2}$	$6.68(26) \times 10^{-2}$	$6.55(72) \times 10^{-2}$	$6.66(26) \times 10^{-2}$
$9^3S \rightarrow 11^3P$	$1.272(30) \times 10^{-2}$	$1.247(20) \times 10^{-2}$	$1.266(30) \times 10^{-2}$	$1.243(20) \times 10^{-2}$
$2^3P \rightarrow 10^3S$	$3.171\,40(56) \times 10^{-4}$	$3.171\,11(98) \times 10^{-4}$	$3.168\,75(56) \times 10^{-4}$	$3.168\,48(98) \times 10^{-4}$
$3^3P \rightarrow 10^3S$	$9.2078(62) \times 10^{-4}$	$9.2061(43) \times 10^{-4}$	$9.2005(62) \times 10^{-4}$	$9.1986(43) \times 10^{-4}$
$4^3P \rightarrow 10^3S$	$2.0037(28) \times 10^{-3}$	$2.0032(12) \times 10^{-3}$	$2.0022(28) \times 10^{-3}$	$2.0017(12) \times 10^{-3}$
$5^3P \rightarrow 10^3S$	$4.126(12) \times 10^{-3}$	$4.123(19) \times 10^{-3}$	$4.123(12) \times 10^{-3}$	$4.1177(19) \times 10^{-3}$
$6^3P \rightarrow 10^3S$	$8.834(43) \times 10^{-3}$	$8.7943(93) \times 10^{-3}$	$8.825(43) \times 10^{-3}$	$8.7862(93) \times 10^{-3}$
$7^3P \rightarrow 10^3S$	$2.173(31) \times 10^{-2}$	$2.1705(31) \times 10^{-2}$	$2.171(31) \times 10^{-2}$	$2.1681(31) \times 10^{-2}$
$8^3P \rightarrow 10^3S$	$7.666(92) \times 10^{-2}$	$7.682(23) \times 10^{-2}$	$7.668(92) \times 10^{-2}$	$7.673(23) \times 10^{-2}$
$9^3P \rightarrow 10^3S$	$9.700(51) \times 10^{-1}$	$9.718(18) \times 10^{-1}$	$9.701(51) \times 10^{-1}$	$9.712(18) \times 10^{-1}$
$10^3S \rightarrow 5^3P$	4.15(13)	4.162(11)	4.13(13)	4.176(11)
$10^3S \rightarrow 11^3P$	$7.910(81) \times 10^{-2}$	$7.917(60) \times 10^{-2}$	$7.909(81) \times 10^{-2}$	$7.894(60) \times 10^{-2}$
$2^3P \rightarrow 11^3S$	$2.3126(19) \times 10^{-4}$	$2.3133(24) \times 10^{-4}$	$2.3099(19) \times 10^{-4}$	$2.3106(24) \times 10^{-4}$
$3^3P \rightarrow 11^3S$	$6.5561(59) \times 10^{-4}$	$6.5523(64) \times 10^{-4}$	$6.5487(59) \times 10^{-4}$	$6.5445(64) \times 10^{-4}$
$4^3P \rightarrow 11^3S$	$1.3687(13) \times 10^{-3}$	$1.3681(13) \times 10^{-3}$	$1.3672(13) \times 10^{-3}$	$1.3664(13) \times 10^{-3}$
$5^3P \rightarrow 11^3S$	$2.6465(61) \times 10^{-3}$	$2.6397(41) \times 10^{-3}$	$2.6442(61) \times 10^{-3}$	$2.6365(41) \times 10^{-3}$
$6^3P \rightarrow 11^3S$	$5.092(41) \times 10^{-3}$	$5.0734(53) \times 10^{-3}$	$5.088(41) \times 10^{-3}$	$5.0684(53) \times 10^{-3}$
$7^3P \rightarrow 11^3S$	$1.0392(74) \times 10^{-2}$	$1.0410(25) \times 10^{-2}$	$1.0375(74) \times 10^{-2}$	$1.0396(25) \times 10^{-2}$
$8^3P \rightarrow 11^3S$	$2.516(48) \times 10^{-2}$	$2.508(14) \times 10^{-2}$	$2.515(48) \times 10^{-2}$	$2.504(14) \times 10^{-2}$
$9^3P \rightarrow 11^3S$	$8.65(37) \times 10^{-2}$	$8.772(79) \times 10^{-2}$	$8.62(37) \times 10^{-2}$	$8.760(79) \times 10^{-2}$
$10^3P \rightarrow 11^3S$	1.095(71)	1.091(35)	1.099(71)	1.082(35)
$11^3S \rightarrow 11^3P$	4.56(11)	4.59(12)	4.56(11)	4.59(12)
$2^3P \rightarrow 12^3S$	$1.747(13) \times 10^{-4}$	$1.748(15) \times 10^{-4}$	$1.746(13) \times 10^{-4}$	$1.747(15) \times 10^{-4}$
$3^3P \rightarrow 12^3S$	$4.859(29) \times 10^{-4}$	$4.851(28) \times 10^{-4}$	$4.852(29) \times 10^{-4}$	$4.847(28) \times 10^{-4}$
$4^3P \rightarrow 12^3S$	$9.854(68) \times 10^{-4}$	$9.844(67) \times 10^{-4}$	$9.843(68) \times 10^{-4}$	$9.833(67) \times 10^{-4}$
$5^3P \rightarrow 12^3S$	$1.820(12) \times 10^{-3}$	$1.814(12) \times 10^{-3}$	$1.817(12) \times 10^{-3}$	$1.813(12) \times 10^{-3}$
$6^3P \rightarrow 12^3S$	$3.269(40) \times 10^{-3}$	$3.259(21) \times 10^{-3}$	$3.265(40) \times 10^{-3}$	$3.256(21) \times 10^{-3}$
$7^3P \rightarrow 12^3S$	$5.998(38) \times 10^{-3}$	$6.017(44) \times 10^{-3}$	$5.989(38) \times 10^{-3}$	$6.011(44) \times 10^{-3}$
$8^3P \rightarrow 12^3S$	$1.2115(76) \times 10^{-2}$	$1.2041(56) \times 10^{-2}$	$1.2095(76) \times 10^{-2}$	$1.2017(56) \times 10^{-2}$
$9^3P \rightarrow 12^3S$	$2.92(17) \times 10^{-2}$	$2.856(26) \times 10^{-2}$	$2.93(17) \times 10^{-2}$	$2.843(26) \times 10^{-2}$
$10^3P \rightarrow 12^3S$	$1.03(18) \times 10^{-1}$	$9.91(59) \times 10^{-2}$	$1.04(18) \times 10^{-1}$	$9.79(59) \times 10^{-2}$
$11^3P \rightarrow 12^3S$	1.220(66)	1.220(11)	1.220(66)	1.219(11)

The calculated oscillator strengths exhibit a distinct pattern, with the largest values occurring for the $n\,^3S \rightarrow n\,^3P$ and $n\,^3S \rightarrow (n \pm 1)\,^3P$ transitions (i.e., between adjacent states), while much smaller values occurring for transitions between states with significantly different total energies. Based on this pattern, one can envision preparing a beryllium atom in a specific excited Rydberg state through an excitation cascade, such as $3\,^3S \rightarrow 3\,^3P$, $3\,^3P \rightarrow 4\,^3S$, ... While the Rabi frequency, Ω, is the figure of merit in laser-driven population transfer, it scales directly with the transition dipole moment, μ_{if}. Therefore, our oscillator strength survey identifies the transitions that will exhibit the highest Ω for a fixed field amplitude, justifying the proposed cascade event in a coherent excitation experiment. The data obtained in this work can be applied to model light emission and absorption processes involving beryllium atoms in laboratory experiments and interstellar environments. Such models require precise values of the transition energies and oscillator strengths, which this study provides.

ACKNOWLEDGMENTS

This work has been supported by the National Science Foundation (Grant No. 1856702) and Nazarbayev University (FDCRGP Grant No. 040225FD4706). Authors acknowledge the use of high performance computer facilities at the University of Arizona and the Nazarbayev University. We thank Prof. Gordon Drake (University of Windsor) for useful communications and clarifications regarding the oscillator strengths.

DATA AVAILABILITY

The data that support the findings of this article are not publicly available. The data are available from the authors upon reasonable request.

APPENDIX: OSCILLATOR STRENGTH FOR A TRANSITION BETWEEN MULTIPLET STATES

For a multiplet state, the oscillator strength between initial (n_i) and final (n_f) levels is defined as follows:

$$f_{if}^{\text{multiplet}} = \frac{1}{\sum_{J_i}(2J_i+1)\Delta\overline{E}_{if}} \sum_{J_i,J_f}(2J_i+1)\Delta E_{J_iJ_f} f_{J_iJ_f}, \tag{A1}$$

where J_i and J_f are the total angular momentum quantum numbers of the initial (i) and final (f) states, respectively. The mean transition energy for the multiplet, $\Delta\overline{E}_{if}$, may be obtained from the weighted energy levels. Often the energy differences for the lines within a multiplet are small, in which case the calculation of the mean transition energy can be simplified [53]. In this work it has been assumed that $\Delta\overline{E}_{if} \approx \Delta E_{J_iJ_f}$.

In this Appendix, for precision, we outline the procedure used to calculate the oscillator strength in the length gauge. The procedure for the velocity gauge is similar. Notably, for the latter, Eq. (A2) and the transition dipole moment operator must be appropriately modified [see Eqs. (6) and (9)]. The oscillator strength in the length gauge between initial (J_i) and final (J_f) states is defined as [4,32,33]

$$f^{\text{L}}_{J_iJ_f} = \frac{2}{3\,g_i}\Delta E_{J_iJ_f}\, S^{\text{L}}_{J_iJ_f}, \tag{A2}$$

where $\Delta E_{J_iJ_f} = E_f - E_i$ is the transition energy, $g_i = 2J_i + 1$ is the statistical weight of the initial state, and $S^{\text{L}}_{J_iJ_f}$ is the line strength in the length gauge.

For a Coulombic system, the line strength for the $|n_i\,L_i\,S_i\,J_i\,M_i\rangle \to |n_f\,L_f\,S_f\,J_f\,M_f\rangle$ transition is defined by

$$S^{\text{L}}_{J_iJ_f} = \sum_{M_i,M_f} |\langle n_i\,L_i\,S_i\,J_i\,M_i|\boldsymbol{\mu}^{\text{L}}|n_f\,L_f\,S_f\,J_f\,M_f\rangle|^2, \tag{A3}$$

where $\boldsymbol{\mu}^{\text{L}}$ is the transition dipole moment operator in the length formalism. Using the Wigner-Eckart theorem, $S^{\text{L}}_{J_iJ_f}$ (A3) can be related to the reduced matrix element by (for more information see Sec. 2.8 of Ref. [33])

$$S^{\text{L}}_{J_iJ_f} = |\langle n_i\,L_i\,S_i\,J_i\,M_i||\boldsymbol{\mu}^{\text{L}}||n_f\,L_f\,S_f\,J_f\,M_f\rangle|^2 \times \sum_{M_i,k,M_f}\left|\begin{pmatrix} J_i & 1 & J_f \\ -M_i & k & M_j\end{pmatrix}\right|^2, \tag{A4}$$

where $\langle n_i\,L_i\,S_i\,J_i\,M_i||\boldsymbol{\mu}^{\text{L}}||n_f\,L_f\,S_f\,J_f\,M_f\rangle$ is the reduced matrix element which is independent on the angular-momentum-projection quantum numbers, M_i and M_j, and k is equal to 3 for the three components of the transition dipole moment operator (μ^{L}_x, μ^{L}_y, μ^{L}_z). The reduced matrix element encodes the radial part of the transition and is defined within the spherical tensor formalism according to the Wigner-Eckart theorem. This factor isolates the angular dependence via Clebsch-Gordan coefficients or $3j$ symbols [second term of Eq. (A4)], while the radial dependence is computed numerically from the corresponding wavefunctions. Using the sum rule for the $3j$ symbols,

$$\sum_{k,M_i,M_f}\left|\begin{pmatrix} J_i & 1 & J_f \\ -M_i & k & M_j\end{pmatrix}\right|^2 = 1. \tag{A5}$$

It can be seen that the line strength is identical to the reduced matrix element:

$$S^{\text{L}}_{J_iJ_f} = |\langle n_i\,L_i\,S_i\,J_i\,M_i||\boldsymbol{\mu}^{\text{L}}||n_f\,L_f\,S_f\,J_f\,M_f\rangle|^2. \tag{A6}$$

For a nonrelativistic calculation in the LS coupling scheme, $S_i = S_f$ and we can strip out the dependence on J_i and J_f (see chapter 7 of Ref. [59] and see chapters 10 and 11 of Ref. [33]) to obtain

$$S^{\text{L}}_{J_iJ_f} = \left|(-1)^{L_i+S_f+J_f+1} \times [(2J_f+1)(2J_i+1)]^{1/2} \times \begin{Bmatrix} L_i & J_i & S_f \\ J_f & L_f & 1\end{Bmatrix} \times \langle n_i\,L_i||\boldsymbol{\mu}^{\text{L}}||n_f\,L_f\rangle\right|^2, \tag{A7}$$

where $\langle n_i\,L_i||\boldsymbol{\mu}^{\text{L}}||n_f\,L_f\rangle$ is the reduced matrix element if spin is neglected and curly brackets denote $6j$ symbol. To calculate the reduced matrix element, the following formula can be uses in accord with the Wigner-Eckart theorem:

$$\langle n_i\,L_i||\boldsymbol{\mu}^{\text{L}}||n_f\,L_f\rangle = \frac{(-1)^{L_i}\langle n_iL_i|\mu^{\text{L}}_z|n_fL_f\rangle}{\begin{pmatrix} L_i & 1 & L_f \\ 0 & 0 & 0\end{pmatrix}}. \tag{A8}$$

For the $S \to P$ and $P \to S$ transitions considered in this work, the $3j$ coefficients become, respectively,

$$\begin{pmatrix} 0 & 1 & 1 \\ 0 & 0 & 0\end{pmatrix} = -\frac{1}{\sqrt{3}}, \quad \begin{pmatrix} 1 & 1 & 0 \\ 0 & 0 & 0\end{pmatrix} = -\frac{1}{\sqrt{3}}. \tag{A9}$$

So Eq. (A8) can be written in the following form:

$$\langle n_i\,L_i||\boldsymbol{\mu}^{\text{L}}||n_f\,L_f\rangle = -\sqrt{3} \times (-1)^{L_i+1}\langle n_iL_i|\mu^{\text{L}}_z|n_fL_f\rangle. \tag{A10}$$

[1] R. L. Kurucz, Atomic data for interpreting stellar spectra: Isotopic and hyperfine data, Phys. Scr. **T47**, 110 (1993).

[2] J. Tennyson, S. N. Yurchenko, A. F. Al-Refaie, V. H. Clark, K. L. Chubb, E. K. Conway, A. Dewan, M. N. Gorman, C. Hill, A. Lynas-Gray, T. Mellor, L. K. McKemmish, A. Owens, O. L. Polyansky, M. Semenov, W. Somogyi, G. Tinetti, A. Upadhyay, I. Waldmann, Y. Wang *et al.*, The 2020 release of the exomol database: Molecular line lists for exoplanet and other hot atmospheres, J. Quant. Spectrosc. Radiat. Transfer **255**, 107228 (2020).

[3] J. E. Sansonetti and W. C. Martin, Handbook of basic atomic spectroscopic data, J. Phys. Chem. Ref. Data **34**, 1559 (2005).

[4] W. C. Martin, W. L. Wiese, and A. Kramida, Atomic spectroscopy, in *Springer Handbook of Atomic, Molecular, and*

Optical Physics, edited by G. W. F. Drake (Springer, New York, 2023), pp. 177–197.

[5] P. F. Bernath, *Spectra of Atoms and Molecules*, 5th ed. (Oxford University Press, New York, 2025).

[6] P. A. M. Dirac and R. H. Fowler, Quantum mechanics of many-electron systems, Proc. R. Soc. London A **123**, 714 (1929).

[7] G. W. F. Drake, High precision calculations for helium, in *Springer Handbook of Atomic, Molecular, and Optical Physics*, edited by G. W. F. Drake (Springer, New York, 2023), pp. 199–216.

[8] S. Nasiri, S. Bubin, and L. Adamowicz, Non-Born–Oppenheimer variational calculations of atoms and molecules with explicitly correlated Gaussian basis functions, in *Chemical Physics and Quantum Chemistry*, Advances in Quantum Chemistry Vol. 81, edited by K. Ruud and E. J. Brändas (Academic Press, Amsterdam, 2020), pp. 143–166.

[9] T. Kato, On the eigenfunctions of many-particle systems in quantum mechanics, Commun. Pure Appl. Math. **10**, 151 (1957).

[10] Y. I. Kurokawa, H. Nakashima, and H. Nakatsuji, General coalescence conditions for the exact wave functions: Higher-order relations for two-particle systems, J. Chem. Phys. **139**, 044114 (2013).

[11] S. Bubin, M. Pavanello, W.-C. Tung, K. L. Sharkey, and L. Adamowicz, Born–Oppenheimer and non-Born–Oppenheimer, atomic and molecular calculations with explicitly correlated Gaussians, Chem. Rev. **113**, 36 (2013).

[12] S. Bubin and L. Adamowicz, Matrix elements of N-particle explicitly correlated Gaussian basis functions with complex exponential parameters, J. Chem. Phys. **124**, 224317 (2006).

[13] S. Bubin and L. Adamowicz, Energy and energy gradient matrix elements with N-particle explicitly correlated complex Gaussian basis functions with $L = 1$, J. Chem. Phys. **128**, 114107 (2008).

[14] T. Shomenov and S. Bubin, Explicitly correlated Gaussians for high-precision variational calculations of S^e, P^e, and D^e states of quantum systems: An efficient algorithm, Phys. Rev. E **108**, 065308 (2023).

[15] S. Nasiri, L. Adamowicz, and S. Bubin, Benchmark calculations of the energy spectra and oscillator strengths of the beryllium atom, J. Phys. Chem. Ref. Data **50**, 043107 (2021).

[16] M. Stanke, A. Kędziorski, and L. Adamowicz, Fine structure of the beryllium ^3P states calculated with all-electron explicitly correlated Gaussian functions, Phys. Rev. A **105**, 012813 (2022).

[17] S. Nasiri, J. Liu, S. Bubin, M. Stanke, A. Kędziorski, and L. Adamowicz, Oscillator strengths and interstate transition energies involving ^2S and ^2P states of the Li atom, At. Data Nucl. Data Tables **149**, 101559 (2023).

[18] S. Nasiri, S. Bubin, and L. Adamowicz, Oscillator strengths for $^2P - ^2S$ transitions in neutral boron, Phys. Rev. A **109**, 042813 (2024).

[19] D. Tumakov, P. Rzhevskii, T. Shomenov, and S. Bubin, Relativistic corrections in the ground and excited states of positronic beryllium, Phys. Rev. A **109**, 042826 (2024).

[20] S. Nasiri, D. Tumakov, M. Stanke, A. Kedziorski, L. Adamowicz, and S. Bubin, Fine structure of the doublet P levels of boron, Phys. Rev. Res. **6**, 043225 (2024).

[21] I. Hornyák, L. Adamowicz, and S. Bubin, Low-lying ^2S states of the singly charged carbon ion, Phys. Rev. A **102**, 062825 (2020).

[22] M. Stanke, A. Kędziorski, S. Nasiri, L. Adamowicz, and S. Bubin, Fine structure of the ^2P energy levels of singly ionized carbon (C II), Phys. Rev. A **108**, 012812 (2023).

[23] D. Kondratyev, L. Vainshtein, I. Bray, D. Fursa, and Y. Ralchenko, Atomic data and collisional–radiative model for beryllium and its ions, Phys. Scr. **T161**, 014007 (2014).

[24] W. D. Williams (private communication).

[25] S. Brezinsek, M. Stamp, D. Nishijima, D. Borodin, S. Devaux, K. Krieger, S. Marsen, M. O'Mullane, C. Bjoerkas, A. Kirschner *et al.*, Study of physical and chemical assisted physical sputtering of beryllium in the JET ITER-like wall, Nucl. Fusion **54**, 103001 (2014).

[26] H. Summers, The ADAS user manual, version 2.6, http://www.adas.ac.uk/ (2004).

[27] R. Li, M. Mostamand, J. Romans, and J. Lassen, Polarization-dependent laser resonance ionization of beryllium, Spectrochim. Acta B **174**, 105998 (2020).

[28] H. P. Summers, W. J. Dickson, A. Boileau, P. G. Burke, B. Denne-Hinnov, W. Fritsch, R. Giannella, N. C. Hawkes, M. von Hellerman, W. Mandl, *et al.*, Spectral emission from beryllium in plasmas, Plasma Phys. Controlled Fusion **34**, 325 (1992).

[29] M. Puchalski, J. Komasa, and K. Pachucki, Testing quantum electrodynamics in the lowest singlet states of the beryllium atom, Phys. Rev. A **87**, 030502(R) (2013).

[30] M. Wang, W. Huang, F. Kondev, G. Audi, and S. Naimi, The AME 2020 atomic mass evaluation (II). Tables, graphs and references, Chin. Phys. C **45**, 030003 (2021).

[31] J. Mitroy, S. Bubin, W. Horiuchi, Y. Suzuki, L. Adamowicz, W. Cencek, K. Szalewicz, J. Komasa, D. Blume, and K. Varga, Theory and application of explicitly correlated Gaussians, Rev. Mod. Phys. **85**, 693 (2013).

[32] A. Hibbert, Atomic structure theory, in *Progress in Atomic Spectroscopy*, edited by W. Hanle and H. Kleinpoppen (Springer, Boston, 1978), pp. 1–69.

[33] G. W. F. Drake, editor, *Springer Handbook of Atomic, Molecular, and Optical Physics* (Springer, New York, 2023).

[34] C. Baxter, Center-of-mass motion of an N-particle atom or ion and the Thomas-Reiche-Kuhn sum rule, Phys. Rev. A **50**, 875 (1994).

[35] B.-L. Zhou, J.-M. Zhu, and Z.-C. Yan, Generalized Thomas-Reiche-Kuhn sum rule, Phys. Rev. A **73**, 014501 (2006).

[36] I. Hornyák, S. Nasiri, S. Bubin, and L. Adamowicz, ^2S Rydberg spectrum of the boron atom, Phys. Rev. A **104**, 032809 (2021).

[37] M. Puchalski, J. Komasa, and K. Pachucki, Fine and hyperfine splitting of the low-lying states of ^{9}Be, Phys. Rev. A **104**, 022824 (2021).

[38] A. M. Frolov and M. B. Ruiz, Bound state spectrum of the triplet states in the Be atom, Chem. Phys. Lett. **595-596**, 197 (2014).

[39] K. T. Chung and X.-W. Zhu, Energies, fine structures, and isotope shifts of the $1s^2 2snl$ excited states of the beryllium atom, Phys. Rev. A **48**, 1944 (1993).

[40] A. M. Frolov and D. M. Wardlaw, Triplet 2^3S states in four-electron be-like ions: Bound-state properties and hyperfine-structure splitting, Phys. Rev. A **79**, 064501 (2009).

[41] C. Chen, Energies, fine structures, and hyperfine structures of the $1s^2 2snp\,^3P(n = 2 - 4)$ states for the beryllium atom, J. Atomic Mol. Phys. **2012**, 569876 (2012).

[42] M. Hamermesh, *Group Theory and Its Application to Physical Problems* (Addison-Wesley, Reading, MA, 1962).

[43] P. J. Mohr, D. B. Newell, B. N. Taylor, and E. Tiesinga, CODATA recommended values of the fundamental physical constants: 2022, Rev. Mod. Phys. **97**, 025002 (2025).

[44] J. Mitroy, Polarizabilities of the beryllium clock transition, Phys. Rev. A **82**, 052516 (2010).

[45] C. Froese Fischer and G. Tachiev, Breit–Pauli energy levels, lifetimes, and transition probabilities for the beryllium-like to neon-like sequences, At. Data Nucl. Data Tables **87**, 1 (2004).

[46] M.-K. Chen, The energies and oscillator strengths of bound states of Be, J. Phys. B **31**, 4523 (1998).

[47] D. Bégué, M. Mérawa, and C. Pouchan, Dynamic dipole and quadrupole polarizabilities for the ground 2^1S and the low-lying 3^1S and 3^3S states of Be, Phys. Rev. A **57**, 2470 (1998).

[48] D. Bégué, M. Mérawa, M. Rérat, and C. Pouchan, Dynamic scalar and tensor polarizabilities for the low-lying $2\,^1P^o$ and $2\,^3P^o$ states of Be, J. Phys. B **31**, 5077 (1998).

[49] T. Chang and X. Tang, Oscillator strengths for the bound-bound transitions in beryllium and magnesium, J. Quant. Spectrosc. Radiat. Transfer **43**, 207 (1990).

[50] R. Moccia and P. Spizzo, One-photon transition probabilities and photoionisation cross section calculations of Be, J. Phys. B **18**, 3537 (1985).

[51] E. Markiewicz, R. P. McEachran, and M. Cohen, The polarized frozen-core approximation: Oscillator strengths for the beryllium isoelectronic sequence, Phys. Scr. **23**, 828 (1981).

[52] G. Tachiev and C. Froese Fischer, Breit-Pauli energy levels, lifetimes, and transition data: Beryllium-like spectra, J. Phys. B **32**, 5805 (1999).

[53] J. R. Fuhr and W. L. Wiese, Tables of atomic transition probabilities for beryllium and boron, J. Phys. Chem. Ref. Data **39**, 013101 (2010).

[54] J. Bromander, Lifetimes an oscillator strengths in spectra of Be, B and C, Phys. Scr. **4**, 61 (1971).

[55] H. Kerkhoff, M. Schmidt, and P. Zimmermann, Lifetime measurements in the $2s3s^3S$ and $2s3d^3D$ states of Be I by elective laser excitation, Phys. Lett. A **80**, 11 (1980).

[56] G. Tachiev and C. Froese Fischer, Breit-Pauli energy levels, lifetimes and transition data: Boron-like spectra, J. Phys. B **33**, 2419 (2000).

[57] T. Ishida and K. Ohno, The influence of basis sets on wave function tails, Int. J. Quantum Chem. **35**, 257 (1989).

[58] E. U. Condon and G. H. Shortley, *The Theory of Atomic Spectra* (Cambridge University Press, London, 1935).

[59] A. Edmonds, *Angular Momentum in Quantum Mechanics*, Princeton Landmarks in Mathematics and Physics (Princeton University Press, Princeton, 1996).